Novel Host Proteins and Signaling Pathways in Enteropathogenic *E. coli* Pathogenesis Identified by Global Phosphoproteome Analysis*[S]

Roland Scholz‡, Koshi Imami§, Nichollas E. Scott§, William S. Trimble¶‖, Leonard J. Foster§‡‡, and B. Brett Finlay‡**¶¶‡‡**

Enteropathogenic *Escherichia coli* (EPEC) uses a type III secretion system (T3SS) to directly translocate effector proteins into host cells where they play a pivotal role in subverting host cell signaling needed for disease. However, our knowledge of how EPEC affects host protein phosphorylation is limited to a few individual protein studies. We employed a quantitative proteomics approach to globally map alterations in the host phosphoproteome during EPEC infection. By characterizing host phosphorylation events at various time points throughout infection, we examined how EPEC dynamically impacts the host phosphoproteome over time. This experimental setup also enabled identification of T3SS-dependent and -independent changes in host phosphorylation. Specifically, T3SS-regulated events affected various cellular processes that are known EPEC targets, including cytoskeletal organization, immune signaling, and intracellular trafficking. However, the involvement of phosphorylation in these events has thus far been poorly studied. We confirmed the MAPK family as an established key host player, showed its central role in signal transduction during EPEC infection, and extended the repertoire of known signaling hubs with previously unrecognized proteins, including TPD52, CIN85, EPHA2, and HSP27. We identified altered phosphorylation of known EPEC targets, such as cofilin, where the involvement of phosphorylation has so far been undefined, thus providing novel mechanistic insights into the roles of these proteins in EPEC infection. An overlap of regulated proteins, especially those that are cytoskeleton-associated, was observed when compared with the phosphoproteome of *Shigella*-infected cells. We determined the biological relevance of the phosphorylation of a novel protein in EPEC pathogenesis, septin-9 (SEPT9). Both siRNA knockdown and a phosphorylation-impaired SEPT9 mutant decreased bacterial adherence and EPEC-mediated cell death. In contrast, a phosphorylation-mimicking SEPT9 mutant rescued these effects. Collectively, this study provides the first global analysis of phosphorylation-mediated processes during infection with an extracellular, diarrheagenic bacterial pathogen. *Molecular & Cellular Proteomics 14: 10.1074/mcp.M114.046847, 1927–1945, 2015.*

Diarrheagenic *E. coli* are a major global health burden and cause much morbidity and mortality worldwide. Enteropathogenic *E. coli* (EPEC)[1] is the causative agent of potentially fatal infantile diarrhea and remains an endemic health threat for children in developing countries. EPEC and the closely related enterohemorrhagic *E. coli* (EHEC) belong to the group of at-

From the ‡Michael Smith Laboratories and §Centre for High-Throughput Biology, University of British Columbia, Vancouver, British Columbia V6T 1Z4, Canada, ¶Cell Biology Program, Hospital for Sick Children and ‖Department of Biochemistry, University of Toronto, Toronto, Ontario M5G 1X8, Canada, **Department of Biochemistry and Molecular Biology, University of British Columbia, Vancouver, British Columbia V6T 1Z4, Canada, and ¶¶Department of Microbiology and Immunology, University of British Columbia, Vancouver, British Columbia V6T 1Z4, Canada

Received November 27, 2014, and in revised form, April 22, 2015
Published, MCP Papers in Press, May 5, 2015, DOI 10.1074/mcp.M114.046847

Author contributions: R.S. designed research; R.S., K.I., and N.E.S. performed research; W.S.T., L.J.F., and B.B.F. contributed new reagents or analytic tools; R.S., K.I., N.E.S., and L.J.F. analyzed data; R.S., K.I., N.E.S., L.J.F., and B.B.F. wrote the paper; L.J.F. and B.B.F. share corresponding authorship.

[1] The abbreviations used are: A/E, attaching and effacing; cfu, colony-forming unit; DAVID, Database for Annotation Visualization and Integrated Discovery; DMEM, Dulbecco's modified Eagle medium; *E. coli*, *Escherichia coli*; EPEC, enteropathogenic *Escherichia coli*; FTMS, Fourier transform mass spectrometry; EHEC, enterohemorrhagic *Escherichia coli*; GOTERM_BP_FAT, Gene Ontology Biological Process Functional Annotation Tool; GOTERM_CC_FAT, Gene Ontology Cellular Component Functional Annotation Tool; hpi, hours postinoculation; HPLC, high-performance liquid chromatography; ITMS, ion trap mass spectrometer; KEA, kinase enrichment analysis; KEGG, Kyoto Encyclopedia of Genes and Genomes; LC-MS/MS, liquid-chromatography tandem mass spectrometry; LDH, lactate dehydrogenase; MOI, multiplicity of infection; MS, mass spectrometry; NCBI, National Center for Biotechnology Information; *S. typhimurium, Salmonella enterica* serovar *typhimurium*; *S. flexneri, Shigella flexneri*; SILAC, stable isotope labeling by amino acids in cell culture; SP_PIR, Swiss-Prot and Protein Information Resource; STRING, Search Tool for the Retrieval of Interacting Genes/Proteins; T3S, type III secretion; T3SS, type III secretion system; WT, wild-type.

taching and effacing (A/E) pathogens that form distinct A/E lesions on the surface of intestinal epithelial cells causing the loss of the characteristic intestinal brush border architecture (1).

Upon attachment to intestinal cells, EPEC uses a syringe-like molecular apparatus, the type III secretion system (T3SS), to inject at least 25 unique bacterial effector proteins into the host cell (2–4). Once translocated into mammalian cells, these effectors manipulate a wide range of host signaling pathways, thereby subverting host cell function and promoting virulence (5). The bacterial translocated intimin receptor (Tir) is one of the first and most abundant effectors injected into the host cell: it mediates intimate attachment of EPEC to the enterocyte apical surface via its interaction with the bacterial surface adhesin intimin (6, 7). In concert with other effectors, Tir also provokes an expansive cytoskeletal rearrangement leading to the formation of actin-rich protrusions, termed pedestals, beneath the site of bacterial attachment (8). Besides altering the host cell cytoskeleton, EPEC effectors also manipulate cellular trafficking, host immune response and ion and water homeostasis to cause disease (5). Although significant effort in recent years has led to the identification of multiple key players in both the host and the pathogen, the complex interactions between EPEC and the epithelial host cell, and the underlying molecular mechanisms, are still collectively not well understood.

There is increasing evidence that hijacking host post-translational mechanisms such as protein phosphorylation is a key strategy for bacterial pathogens to efficiently subvert host cell function (9) and there are several indications that this may be the case for EPEC. For example, Tir is phosphorylated upon insertion into the host cell membrane and this event plays a role in the rearrangement of the actin cytoskeleton (10). Another EPEC-encoded effector, NleH, contains a functional kinase domain suggesting the potential of directly phosphorylating host cell targets (11). Moreover, the phosphorylation profiles of a few specific host proteins such as cortactin, CT10 regulator of kinase (CRK) adaptors, focal adhesion kinase (FAK) and mitogen-activated protein kinase 1 (MAPK1), as well as alterations in tyrosine phosphorylation of host proteins, are impacted in an EPEC effector-dependent manner (12–18). These are selective observations though. Thus, a more comprehensive, system-level analysis is needed to better understand how and to what extent EPEC hijacks host cell phosphorylation to cause disease.

Recent advances in quantitative phosphoproteomics have made it possible to successfully profile the changes in host protein phosphorylation following infection by the invasive, diarrheagenic bacterial pathogens *Shigella* and *Salmonella* (19–21). To our knowledge, no such analysis has been reported for a noninvasive, diarrheagenic bacterial pathogen such as EPEC. In this study, we applied a stable isotope labeling by amino acids in cell culture (SILAC)-based (22) quantitative phosphoproteomics approach to assess the impact of EPEC infection on the host cell phosphoproteome. The integration of time course experiments and the use of an EPEC mutant deficient in type III secretion (T3S) provided further insights into the dynamics as well as the effector dependence of these processes. This experimental approach enabled identification of both stable and transient interactions between EPEC bacterial effectors and host proteins. Additional infection studies focusing on a newly identified host target, septin-9, further emphasizes the biological significance of the manipulation of host protein phosphorylation in EPEC pathogenesis.

EXPERIMENTAL PROCEDURES

Plasmids—The coding region of human septin-9 isoform a (SEPT9(a); NP_001106963; alternative nomenclature: SEPT9 transcript variant 1) was amplified by PCR and cloned into the EcoRI and XhoI sites of pCMV-Tag 2B to generate a mammalian expression plasmid encoding N-terminally FLAG-tagged SEPT9(a). Site-directed mutagenesis (QuikChange, Agilent Technologies, Santa Clara, CA) was performed to replace Ser-30 of FLAG-SEPT9(a) with glutamate (FLAG-SEPT9(a)-S30E) and alanine (FLAG-SEPT9(a)-S30A), respectively. Primers are listed in the supplemental Table S1. All plasmids were verified by sequencing.

Cell Culture and SILAC Labeling—HeLa cells (American Type Culture Collection) were cultured in Dulbecco's modified Eagle medium (DMEM) high glucose (Thermo Scientific, Waltham, MA) supplemented with 10% fetal bovine serum (FBS), 1% nonessential amino acids (NEAA) (Gibco) and 1% GlutaMax (Gibco, Thermo Scientific, Waltham, MA). Cells were grown at 5% (v/v) CO_2 and 37 °C. SILAC labeling of HeLa cells was performed in arginine- and lysine-free DMEM (Caisson Laboratories Inc, North Logan, UT.) supplemented with 10% (v/v) dialyzed fetal bovine serum (Invitrogen, Thermo Scientific, Waltham, MA), 1% GlutaMax (Gibco) as well as L-arginine (42 mg/L) and L-lysine (146 mg/L) ("light" label (L), uninfected HeLa) or L-[$^{13}C_6$]arginine (43.5 mg/L) and L-[$^{2}H_4$]lysine (150 mg/L) ("medium" label (M), EPEC Δ*escN*-infected HeLa) or L-[$^{13}C_6$,$^{15}N_4$]arginine (44.5 mg/L) and L-[$^{13}C_6$,$^{15}N_2$]lysine (154 mg/L) ("heavy" label (H), wild-type EPEC-infected HeLa).

Bacterial Strains and Infection—The prototypical EPEC O127:H6 strain E2348/69 and the T3SS-deficient strain EPEC Δ*escN* were used in this study (23, 24). Prior to infection, EPEC grown on Luria-Bertani (LB) agar plates were used to inoculate LB broth. The bacterial culture was incubated overnight at 37 °C in a shaking incubator. The bacterial cultures were centrifuged at 2300 × *g* for 5 min at room temperature. The bacterial pellet was resuspended in prewarmed serum- and antibiotic-free cell culture medium to a density of 8×10^7 bacteria/ml and incubated in a 37 °C incubator with 5% (v/v) CO_2 for 3–4 h. Upon reaching 80–90% confluence HeLa cells were first washed and then incubated with prewarmed serum- and antibiotic-free cell culture medium 2 h prior to infection with EPEC at a multiplicity of infection (MOI) of 20:1. Small volumes of serum- and antibiotic-free cell culture medium were used during infection to accelerate EPEC attachment and promote more synchronized infection conditions. Uninfected cells were treated with prewarmed serum- and antibiotic-free cell culture medium only.

Sample Preparation for Phosphoproteome Analysis—At specified time points postinfection, HeLa cells were washed twice with ice-cold phosphate-buffered saline (PBS) and harvested on ice. Cell lysis was performed similarly to what has been previously described (21). Briefly, cells were resuspended in 50 mM ammonium bicarbonate and 1% (w/v) sodium deoxycholate and boiled for 5 min. $MgCl_2$ was added to a final concentration of 1.5 mM and DNA was digested by

Benzonase endonuclease (Santa Cruz Biotechnology, Dallas, TX) at room temperature for 30 min. After combining the lysates of light, medium and heavy labeled cells (1:1:1), proteins were reduced with 10 mM DTT at room temperature for 30 min and alkylated with 55 mM iodoacetamide at room temperature for 20 min in the dark. Trypsin (Promega, Fitchburg, WI) digestion was performed at a trypsin-to-protein ratio of 1:100 (w/w) under constant agitation at 37 °C for 16 h. Peptides were desalted with C18 StAGE Tips (25). Phosphopeptides were enriched using lactic acid-modified titanium dioxide (GL Sciences, Tokyo, Japan) and consecutively eluted by 5% (v/v) ammonium hydroxide and 0.5% (v/v) pyrrolidine as previously reported (26, 27). Eluted phosphopeptides were desalted with C18 StAGE Tips (25) prior to analysis by LC-MS/MS.

NanoLC-MS/MS Analysis—Phosphopeptides were separated using an 1100 series nanoflow high-performance liquid chromatography (HPLC) instrument (Agilent) equipped with a two column set up. Samples were loaded onto a 2 cm long, 100 μm inner diameter fused silica trap column containing 5.0 μm Aqua C18 beads (Phenomenex, Torrance, CA) for 10 min in buffer A (0.5% acetic acid) at a flow rate of 5 μl/min prior to analytical separation. Analytical separation was accomplished using a 200 mm in length and 75 μm of inner diameter column containing 3 μm ReproSil-Pur C18-AQ material (Dr. Maisch GmbH, Ammerbuch-Entringen, Germany) at a flow rate of 250 nL/min. Both trap and analytical columns were prepared in-house. Peptides were eluted from the analytical column by altering the gradient from 100% buffer A (0.5% acetic acid) to 40% buffer B (0.5% acetic acid, 80% acetonitrile) over 90 min. The eluting peptides were directly infused into an LTQ-Orbitrap Velos mass spectrometer (ThermoFisher Scientific) via ESI. MS and MS/MS information was collected in a data-dependent manner using the following settings: one full scan (resolution 60,000; *m/z* 300–1600) followed by top 15 MS/MS scans using collision-induced dissociation in the linear ion trap mass spectrometer (ITMS; min. signal required: 200, isolation width: 3 Th, normalized collision energy: 35, activation Q: 0.25, activation time: 10 ms) using dynamic exclusion (repeat count: 1, repeat duration: 30 s, exclusion list size: 500, exclusion duration: 60 s). AGC targets of 1×10^6 and 3×10^4 with maximum fill times of 250 and 100 ms were used for MS and MS-MS scans, respectively.

Because of higher sample complexity, peptides for whole proteome analysis were analyzed on the Q Exactive mass spectrometer (ThermoFisher Scientific) coupled to a two-column EASY-nLC1000 system. Trap and analytical column set up were similar as described above, with the analytical column being 400 mm in length and containing 1.9 μm ReproSil-Pur C18-AQ material (Dr. Maisch GmbH). Buffer A (0.1% formic acid) was used for the trap column. Peptides were eluted from the analytical column using 240 min gradient with following conditions: 100% buffer A (0.1% formic acid) to 32% buffer B (0.1% formic acid, 80% acetonitrile) in 210 min, then 32% to 40% buffer B in 10 min followed by increase to 100% buffer B in 5 min and 100% buffer B for an additional 15 min. MS and MS/MS information was collected in a top-10 data-dependent approach switching between MS (resolution 70,000; AGC target of 3×10^6), and HCD MS-MS events (resolution 17,500, 4.5% underfill ratio, AGC target of 1×10^5 with a maximum injection time of 40 ms, an isolation width of 2.2 Th, and an NCE of 28 with 20% stepping).

Data Analysis—Phosphoproteome raw data were analyzed and processed using MaxQuant (v1.2.2.4) (28). Search parameters included two missed cleavage sites, fixed cysteine carbamidomethyl modification, and variable modifications including methionine oxidation, N-terminal protein acetylation, as well as phosphorylation of serine, threonine, and tyrosine. The search multiplicity was set to three with each multiplicity denoting one of the SILAC amino acid combinations (light: arginine-0, lysine-0; medium: L-[$^{13}C_6$]arginine, L-[$^{2}H_4$]lysine; heavy: L-[$^{13}C_6$,$^{15}N_4$]arginine, L-[$^{13}C_6$,$^{15}N_2$]lysine). Searches were performed using the default peptide mass tolerance of 6 ppm for FTMS MS and 0.5 Da for ITMS MS/MS scans. Both the match between runs and the requantify feature of MaxQuant were enabled. Database search was performed using Andromeda (29) against UniProt/Swiss-Prot human (Oct, 2012) plus EPEC O127:H6 strain E2348/69 (Feb, 2010) (a combined total of 94,910 entries) with common serum contaminants and enzyme sequences and a false discovery rate (FDR) of 1% at both peptide and protein level. Isoleucine and leucine were considered as the same amino acid. Phosphorylation sites were ranked according to their phosphorylation localization probabilities (P) as class I ($p > 0.75$), class II ($0.75 > p > 0.5$), and class III sites ($p < 0.5$) (30). Whole proteome data was analyzed and processed in analogous manner using MaxQuant (v1.5.2.8) omitting the inclusion of the variable search parameter for phosphorylation of serine, threonine, and tyrosine. For protein quantification, a minimum of two ratio counts was set. In the whole proteome analysis, EPEC proteins that largely derived from remnants of adherent bacteria were designated as contaminants and excluded from the final data analysis with a protein and peptide FDR of 1% used as above.

SILAC ratios were transformed into $\log_2$ scale and *p* values for changes from the null hypothesis (SILAC ratio 1:1) were calculated. Only protein and phosphopeptide measurements observed in a minimum of two out of three biological replicates were considered for analysis. To provide a broad overview of regulated phosphorylation site and protein candidates during EPEC infection, following criteria were applied: all phosphorylation sites and proteins that showed a statistically significant ($p < 0.05$) change compared with the uninfected control at least at one time point and either an increase or a decrease of 1.5-fold in at least one experiment at that time point were considered to be "regulated" by EPEC (if a SILAC ratio could only be determined in one of the three experiments then that protein was not considered at all). All bioinformatic analysis was performed using this set of regulated phosphosites and proteins. T3SS-dependence for regulated sites and proteins was determined by comparing their H/L SILAC ratios (EPEC WT-infected *versus* uninfected) with their M/L SILAC ratios (EPEC Δ*escN*-infected *versus* uninfected) at each time point based on a minimum of two out of three biological replicates. Phosphosites and proteins were defined as being "T3SS-regulated" when the impact of EPEC WT- and EPEC Δ*escN*-infected on the host phosphoproteome or proteome were significantly different in at least one time point, *i.e.* when a significant difference between H/L and M/L SILAC ratios was observed ($p < 0.05$). A significant increase of H/L SILAC ratios compared with M/L SILAC ratios was considered T3SS-dependent up-regulation, whereas a decrease was defined as T3SS-dependent down-regulation. All others ($p > 0.05$ for all time points) were defined as being "non-T3SS-regulated."

In addition, a core set of high confidence phosphosite candidates and proteins was separately determined from the extended set of regulated sites and proteins described above. This core set only included regulated phosphosites and proteins with *p* values that additionally passed a Benjamini-Hochberg procedure with an FDR of 0.15.

Bioinformatics—If indicated in the figure legend, hierarchical clustering of heat maps using the Pearson correlation distance metric was performed with the software MultiExperiment Viewer (MeV) v4.8 (31). Kinase enrichment analysis (KEA) on the kinase-family level was done using a web-based application tool (http://amp.pharm.mssm.edu/lib/kea.jsp) (32). Phosphorylation sequence motifs were extracted with WebLogo (http://weblogo.berkeley.edu/logo.cgi) (33). Prediction of kinase-specific phosphosites on kinase family level with high threshold setting was performed with the software GPS v2.1.2 (34). Kinase families were ranked as described in the Results section. The protein association network was constructed using STRING v9.1 (Search Tool for the Retrieval of Interacting Genes/Proteins; http://string-

db.org/) at a medium confidence score (35). Pathway enrichment and functional annotations were performed using the Database for Annotation Visualization and Integrated Discovery (DAVID) Functional Annotation Tool v6.7 (http://david.abcc.ncifcrf.gov/) (36, 37).

Real-time PCR—HeLa cells were cultured in six-well plates and infected as described above. RNA was isolated using the RNeasy Mini kit (Qiagen, Valencia, CA) according to the manufacturer's instructions including on-column DNase digestion for complete removal of genomic DNA contamination. cDNA was synthesized from 1 μg template RNA using the QuantiTect reverse transcription kit (Qiagen). Real-time PCR analysis was performed at a final primer concentration of 0.2 μM each using the QuantiTect SYBR green PCR kit (Qiagen) and the 7500 Fast Real-Time PCR System (Applied Biosystems, Thermo Scientific, Waltham, MA). Primers used for real-time PCR analysis are listed in the supplemental Table S1 and were either designed manually or by using NCBI Primer-BLAST (www.ncbi.nlm.nih.gov/tools/primer-blast/). Data were normalized to the expression of the human housekeeping gene glyceraldehyde-3-phosphate dehydrogenase (GAPDH) and septin-9 (SEPT9) expression levels were determined relative to the expression of SEPT9 in uninfected cells.

siRNA Knockdown—HeLa cells were grown in 24-well plates to 30% confluence and transfected for a final concentration of 100 nM siGENOME SMARTpool siRNA targeting human SEPT9 (SEPT9 siRNA) or control siGENOME nontargeting siRNA pool 1 (nt1 siRNA) (Dharmacon/Thermo Scientific). Transfection was performed using Oligofectamine (Invitrogen) according to the manufacturer's instructions. Media were changed 24 h post-transfection. At 48 h post-transfection, cells were either lysed or infected and subjected to subsequent experimental procedures as specified in the Fig. legends.

Transfection—HeLa cells were transiently transfected using FuGENE HD transfection reagent (Promega) according to the manufacturer's instructions at a transfection reagent-to-DNA ratio of 3:1. Low and biologically relevant expression of CMV promoter-driven FLAG-SEPT9 constructs was achieved by transfection of small amounts of DNA (0.05 μg DNA per well of a 12-well plate; adjusted according to multi-well plate size) similar to an earlier publication (38). HeLa cells were assayed 24 h post-transfection.

SDS-PAGE and Immunoblotting—HeLa cells were lysed on ice in Nonidet P-40 lysis buffer (20 mM Tris pH 7.5, 1% (v/v) Nonidet P-40, 150 mM NaCl, 10 mM sodium pyrophosphate, 50 mM NaF) supplemented with cOmplete EDTA-free protease inhibitor mixture (Roche, Basel, Switzerland) and phosphatase inhibitor mixture 2 (Sigma-Aldrich, St. Louis, MO). Lysates were immediately frozen in liquid nitrogen and later thawed and cleared by centrifugation at 16,100 $\times$ *g* for 10 min at 4 °C. Ten to fifteen micrograms of lysate were separated on 12% SDS-polyacrylamide gels and subjected to standard immunoblotting procedure using mouse antiFLAG M2 (1:2000, Sigma-Aldrich), rabbit anticalnexin (1:2000, Enzo Life Sciences, Farmingdale, NY), or rabbit antiSEPT9 (1:800, (39)) antibodies overnight at 4 °C.

Cell Adherence Assay—HeLa cells were seeded, transfected with either siRNA or plasmid DNA and infected with EPEC as described above. Two hours postinfection, cells were washed eight times with PBS+/+ to rinse off nonadherent bacteria. HeLa cells were lysed and adherent bacteria were released by incubation in 1% Triton-X-100 on a rocking platform at room temperature for 10 min. Subsequently, the cell culture plate was vortexed at medium speed for 2 min and dilutions of the respective EPEC containing suspensions were made to 1:100 and 1:1000 and were plated on LB plates. After overnight incubation at 37 °C, the number of EPEC colony-forming units (cfu) was determined.

LDH-release Assay—At specified time points postinfection the release of lactate dehydrogenase (LDH) from HeLa cells as an indicator for cell death was measured using the CytoTox96 nonradioactive cytotoxicity assay (Promega) according to the manufacturer's instructions. LDH-release was calculated according to manufacturer's instructions using uninfected and 100% LDH release controls and normalized as indicated in the figure legends. As reported earlier, LDH release from bacterial strains was not significant and thus was only considered for the time course experiment in Fig. 1*A*, where HeLa cells were exposed to varying numbers of EPEC at different time points because of the increase in EPEC population during infection.

RESULTS

EPEC-mediated Alterations in the Host Epithelial Phosphoproteome Differ between T3SS Effector-dependent and Effector-independent Mechanisms—To analyze the dynamics of the host phosphoproteome during EPEC infection, we assessed it at early, intermediate and late stages of EPEC infection. The early stage infection time point was chosen to capture the initial events following effector translocation; the late stage time point was chosen to capture EPEC-induced cytotoxic effects in the host cell prior to cell death (40); the intermediate stage time point was chosen to capture an ongoing infection prior to significant cytotoxicity. All experiments were conducted in human epithelial (HeLa) cells, a widely used *in vitro* model of EPEC-host interactions (41).

Thirty minutes postinoculation was chosen as the early stage time point because EPEC attachment and effector translocation occur as early as 15 to 30 min postinoculation (7, 42). To determine an appropriate late stage time point when the first cytotoxic effects occur, cytotoxicity-associated release of lactate dehydrogenase (LDH) from HeLa cells was assessed at 0.5 h, 1.5 h, and 3.0 h postinoculation (hpi) with the wild-type EPEC O127:H6 strain E2348/69 (EPEC WT) and the T3SS-deficient strain EPEC Δ*escN*. EPEC Δ*escN* did not induce significant LDH release over 3 h, whereas EPEC WT triggered significantly increased LDH release 3 hpi (Fig. 1*A*). Thus, we defined 3 hpi as the late stage of EPEC infection, which is similar to times used to investigate EPEC effector function in previous studies (43). Finally, the intermediate stage of EPEC infection was defined as 1.5 hpi, a time point at which no significant LDH release was observed but when the majority of effectors are already translocated into the host cytosol (Fig. 1*A*) (42).

To characterize the host phosphoproteome, we utilized SILAC coupled with phosphopeptide enrichment by TiO_2 affinity chromatography (26) and liquid-chromatography tandem mass spectrometry (LC-MS/MS) (Fig. 1*B*). At each time point, the phosphoproteome of uninfected HeLa cells, EPEC WT, and EPEC Δ*escN* infected cells, each labeled with either light (L), heavy (H), and medium (M) amino acids, respectively, were quantified.

From three biological replicates at each time point we identified a total of 1403 unique human phosphopeptides derived from 775 human proteins with a false discovery rate of 1% at both the peptide and protein level. We defined "regulated phosphosites" based on two criteria: (1) a significant ($p < 0.05$) change in abundance compared with the uninfected

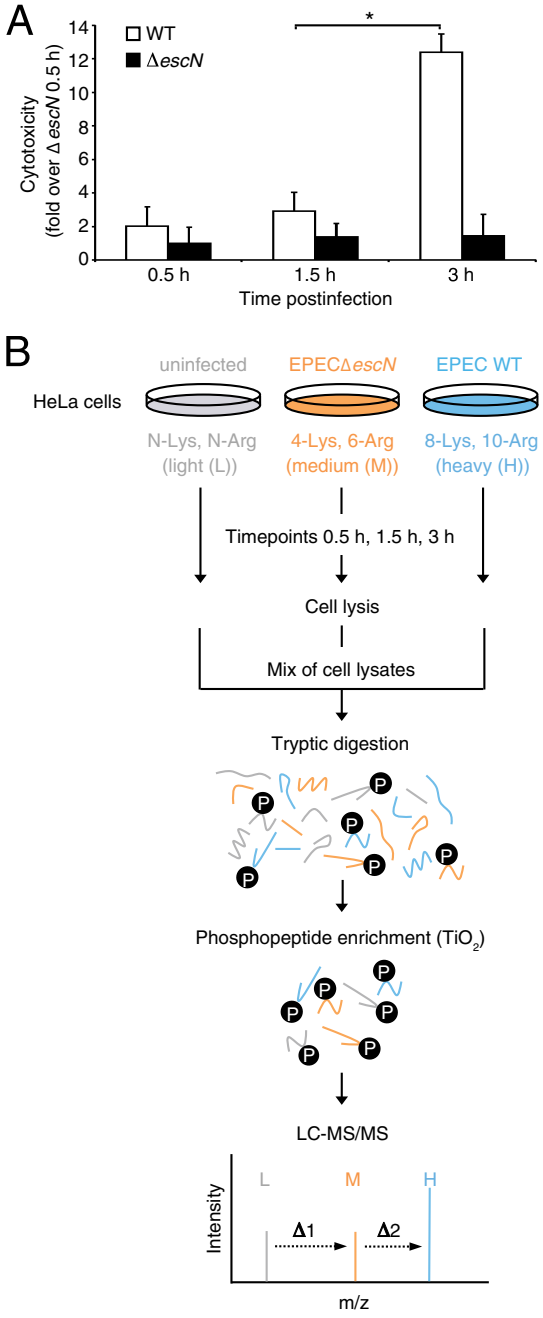

FIG. 1. **Experimental setup for quantitative host phosphoproteome profiling.** *A*, LDH-release assay of EPEC WT- and Δ*escN*-infected HeLa cells to define optimal experimental time points. At indicated time points postinfection, LDH-release as an indicator for cytotoxicity was determined and normalized relative to LDH-release of EPEC Δ*escN*-infected HeLa cells at 0.5 hpi ($n = 3$; +S.D.; *, $p < 0.05$). *B*, Workflow of comparative SILAC-based quantitative proteomic analysis targeting the phosphoproteomes of uninfected, EPEC Δ*escN*- and WT-infected HeLa cells at early, intermediate and late time points postinfection.

control in at least one time point and (2) a ≥1.5-fold change in abundance in at least one experiment at the time point at which a significant change in abundance between infected and uninfected cells was observed (supplemental Table S2). This set of regulated phosphosites was used for the subsequent bioinformatic analysis. In addition we performed a Benjamini-Hochberg multiple hypothesis testing correction to define a core set of particularly high confidence phosphosite candidates (supplemental Table S3). For both EPEC WT- and Δ*escN*-infected cells, the number of regulated phosphosites increased during the course of infection (Fig. 2*A*). Compared with EPEC Δ*escN*-infected cells, EPEC WT-infected cells revealed a greater number of regulated phosphosites; deriving from 110 unique phosphoproteins a total of 129 regulated phosphosites were detected in EPEC WT-infected HeLa cells compared with 77 in EPEC Δ*escN*-infected cells (Fig. 2*B*, upper panel). In both WT- and Δ*escN*-infected cells, protein dephosphorylation was more common than phosphorylation, especially early during infection (Fig. 2*A*). EPEC-induced protein dephosphorylation was described in an earlier study using Western blot analysis with antiphosphotyrosine antibodies (18). However, consistent with other global analysis of eukaryotic phosphorylation (19, 30, 44), phosphorylation at serine and threonine residues, rather than tyrosine, comprised the vast majority of identified phosphosites and EPEC-regulated phosphosites in this study (Fig. 2*B*, center panel). In addition, 27% of protein groups contained multiple regulated phosphosites and thus may serve as complex signaling platforms during EPEC infection (Fig. 2*B*, lower panel).

To determine which phosphosites were regulated in a T3SS effector-dependent or -independent manner, the triplex SILAC experiment enabled the comparison of EPEC WT-infected, EPEC Δ*escN*-infected and uninfected HeLa cells. Phosphosites that displayed similar regulation in both EPEC WT- and Δ*escN*-infected cells were defined as non-T3SS-regulated. Sites with a different regulation pattern between WT- and Δ*escN*-infected cells were defined as T3SS-regulated (see Experimental Procedures). Eighty-nine phosphosites were T3SS-regulated (Table I) and 72 sites were non-T3SS-regulated (supplemental Tables S2 and S4). A heat map representation of SILAC ratios from both T3SS-regulated and non-T3SS-regulated phosphosites enables the visualization of the EPEC-mediated changes in host phosphorylation in a time-dependent manner (Fig. 2*C*). The two highly similar heat maps in the left panel illustrate that non-T3SS-regulated phosphosites undergo similar changes at all time points in EPEC WT- and Δ*escN*-infected cells. In contrast, the heat map profile revealed clear differences for T3SS-regulated sites between WT- and Δ*escN*-infected cells over the course of infection (right panel).

To test whether changes in phosphorylation might be actually because of changes in protein expression we also measured alterations of protein abundance at each time point postinfection (supplemental Tables S6 and S7). The proteome profiles for both EPEC WT- and EPEC Δ*escN*-infected cells were relatively stable over the course of infection with only minor alterations in protein abundance at later time points of

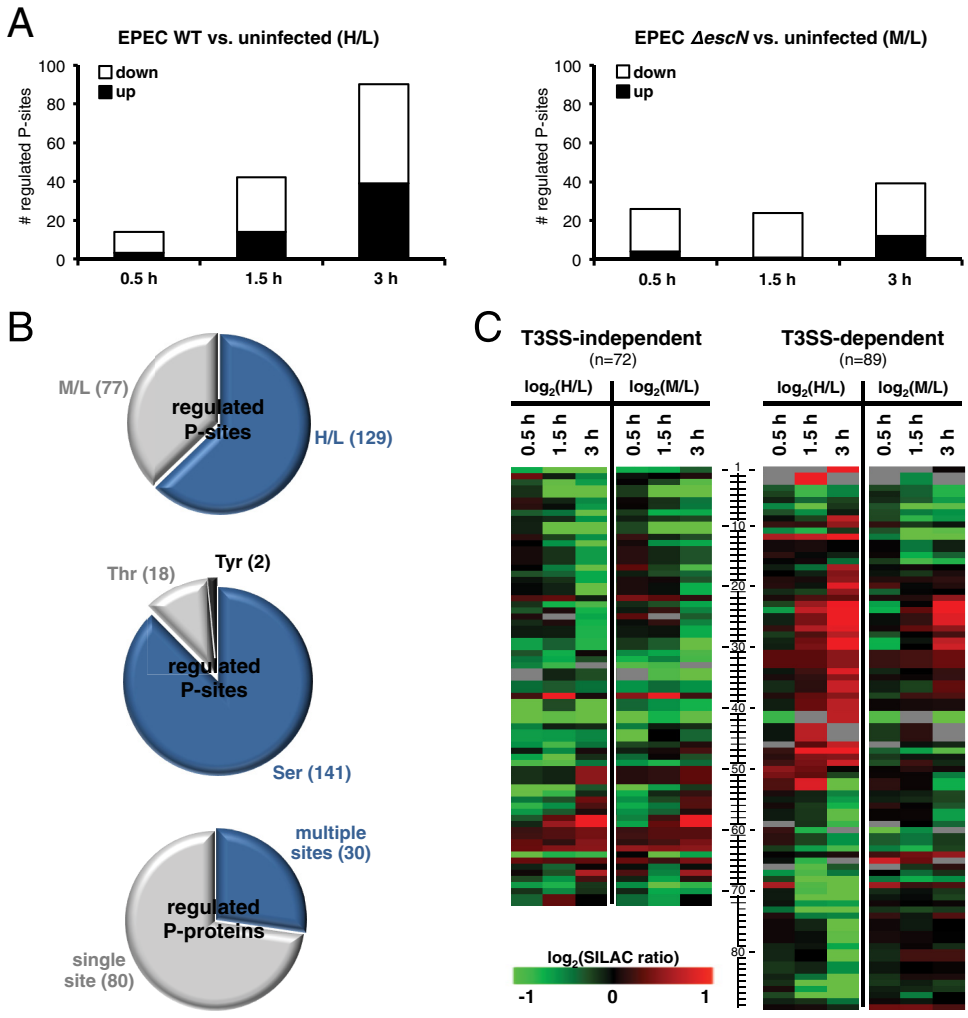

FIG. 2. **Phosphoproteomic analysis of EPEC-infected HeLa cells.** *A*, Temporal distribution of up- (in black) and down-regulated (in white) phosphosites in EPEC WT- and Δ*escN*-infected HeLa cells when each compared with the uninfected control. Respective SILAC label ratios are depicted in parenthesis. Phosphosites were considered regulated when a statistically significant change compared with the uninfected control was detected at least at one time point ($p < 0.05$) and when that change was greater than 1.5-fold in at least one experiment at respective time point. *B, upper panel*, Pie chart representation of the total number of regulated phosphosites in EPEC WT- (in blue, SILAC ratio H/L) and EPEC Δ*escN*-infected HeLa cells (in gray, SILAC ratio M/L) from 0.5 to 3 hpi when each compared with the uninfected control. Phosphosites that were regulated in both conditions were attributed to the total number of each condition. *Center panel*, Distribution of serine (in blue), threonine (in light gray), and tyrosine phosphorylation (in dark gray) based on a total of 161 detected regulated phosphosites. *Lower panel*, Pie chart representation of phosphoproteins with multiple regulated (in blue) and single regulated phosphosites (in gray) based on a total of 110 unique regulated phosphoproteins in EPEC WT- and Δ*escN*-infected HeLa cells from 0.5 to 3 hpi. *C*, Temporal dynamics of T3SS-independently and -dependently regulated phosphosites plotted as a heat map. Phosphosites were defined as T3SS-regulated when the $\log_2$-transformed H/L SILAC ratio revealed a statistical significant difference from the $\log_2$-transformed M/L SILAC ratio. All others were defined as non-T3SS-regulated phosphosites. Each box represents the average of the indicated SILAC ratio at the indicated time point. As depicted in the legend, green represents a decrease in phosphorylation and red represents an increase in phosphorylation when compared with uninfected cells. Dark-shaded boxes indicate no regulation, whereas gray boxes were used when no quantification was available. Heat maps were clustered as described in the experimental procedures. The order of the phosphosites is indicated at the central axis and refers to a phosphosite identifier as depicted in supplemental Table S5.

infection (supplemental Fig. S1). From a total of 2361 identified unique proteins only 1.7% (40 proteins) were considered regulated using the same regulation criteria as for the phosphoproteome analysis (supplemental Fig. S2*A*). The identified proteome overlapped with 34% of the identified phosphoproteome (265 proteins) and with 42% of the regulated phosphoproteome (46 proteins). No overlap was observed between the regulated proteome and the regulated phosphoproteome (supplemental Fig. S2*A*). Among the majority of the overlapping 46 regulated phosphoproteins the observed protein abundances did not correlate with the changes observed in phosphorylation (supplemental Fig. S2*B*). This supports the

TABLE I

*EPEC T3SS-dependently regulated host phosphorylation (selected proteins) *, class II phosphosites (all others class I); all nonisoform-specific entries refer to the canonical sequence of the Swiss-Prot entry in UniProt; +, T3SS-dependent increase (H/L > M/L); -, T3SS-dependent decrease (H/L < M/L); in regular +/−: trend, that is, phosphosite passed either "regulated"-criteria but p(H/L vs. M/L) > 0.05 at respective time point or opposite*

Uniprot ID	Protein name	Gene	Phosphosite	Regulation		
				0.5 h	1.5 h	3 h
Q8WWM7	Ataxin-2-like protein	ATXN2L	S559*	-		
Q13557	Calcium\calmodulin-dependent protein kinase type II subunit delta	CAMK2D	T336*			+
Q05682–4	Caldesmon (isoform 4)	CALD1	S207	+		
P20810	Calpastatin	CAST	S366	+		-
Q15642	Cdc42-interacting protein 4	TRIP10	S296		-	-
Q5SW79	Centrosomal protein of 170 kDa	CEP170	S1112		+	+
Q8WUX9	Charged multivesicular body protein 7	CHMP7	S417			-
P09496	Clathrin light chain A	CLTA	S105	+	+	+
Q9Y281	Cofilin-2	CFL2	S3	+		
P47712	Cytosolic phospholipase A2	PLA2G4A	S729		+	+
P29317	Ephrin type-A receptor 2	EPHA2	T773*		-	
P04792	Heat shock protein beta-1	HSPB1	S82	+	+	+
Q8WWI1–3	LIM domain only protein 7 (isoform 3)	LMO7	S342		-	-
P49006	MARCKS-related protein	MARCKSL1	S22	-	-	
P46821	Microtubule-associated protein 1B	MAP1B	S1396/S1400			-
			S1793*/1797			-
P28482	Mitogen-activated protein kinase 1	MAPK1	Y187	+		
O75970	Multiple PDZ domain protein	MPDZ	S483		-	-
Q09666	Neuroblast differentiation-associated protein AHNAK	AHNAK	S135/S5110		-	-
			S216		+	+
Q96TA1	Niban-like protein 1	FAM129B	S692/S696	-	-	-
A1L390	Pleckstrin homology domain-containing family G member 3	PLEKHG3	S1037/S1040		-	-
Q15149	Plectin	PLEC	S4613/S4622*/T4623*		+	
Q86TB9	Protein PAT1 homolog 1	PATL1	S179		+	+
O94885	SAM and SH3 domain-containing protein 1	SASH1	S813		-	-
Q9UHD8	Septin-9	SEPT9	S30	+	+	+
Q13501	Sequestosome-1	SQSTM1	S272/T269	+		-
Q96B97	SH3 domain-containing kinase-binding protein 1	SH3KBP1	S230		-	-
Q14247	Src substrate cortactin	CTTN	Y421			+
O00161	Synaptosomal-associated protein 23	SNAP23	S110		+	
Q12933	TNF receptor-associated factor 2	TRAF2	T7/S11		+	
Q9BUZ4	TNF receptor-associated factor 4	TRAF4	S426			-
P55327	Tumor protein D52	TPD52	S176	+	+	+
Q5JSH3	WD repeat-containing protein 44	WDR44	S96			+

alteration of phosphopeptide levels predominantly being driven by kinase and phosphatase activities in response to EPEC infection. This said, we cannot fully exclude that alterations in the phosphorylation profile of some specific proteins, especially the ones not identified in the whole proteome analysis, might be also driven by changes in protein expression.

Collectively, these results reveal that EPEC's impact on the host phosphoproteome is much more extensive than previously thought.

Several Kinase Families Modulate Host Phosphorylation during EPEC Infection—Kinases are pivotal regulators of phosphorylation dynamics in cellular signaling and in turn are often regulated by phosphorylation. Therefore, we examined the data for kinases that might play a key role in mediating some of the observed changes seen in the host phosphoproteome during EPEC infection. A total of 36 kinases were identified and quantified in the phosphoproteome analysis (Fig. 3*A*) (supplemental Table S8). Our research identified six kinases with modified phosphorylation following EPEC infection, including the non-T3SS-regulated protein kinase C alpha (PKCα) and the T3SS-regulated calcium/calmodulin-dependent protein kinase type II subunit delta (CAMK2δ), ephrin type-A receptor 2 (EPHA2), and mitogen-activated protein kinase 1 (MAPK1/ERK2) (Fig. 3*A*).

Phosphorylation of Thr-497 in PKCα is critical for kinase activity (45). Its respective phosphopeptide decreased in abundance in infected cells, suggesting that EPEC may reduce PKCα activity upon infection. Consistent with this observation is a previous report showing that cytosolic PKCα activity was decreased in HeLa cells following EPEC infection at early time points (46). However the same study also showed that membrane-bound PKCα activity increased upon EPEC infection, suggesting that the respective membrane-associated PKCα could not be observed in our experimental setup.

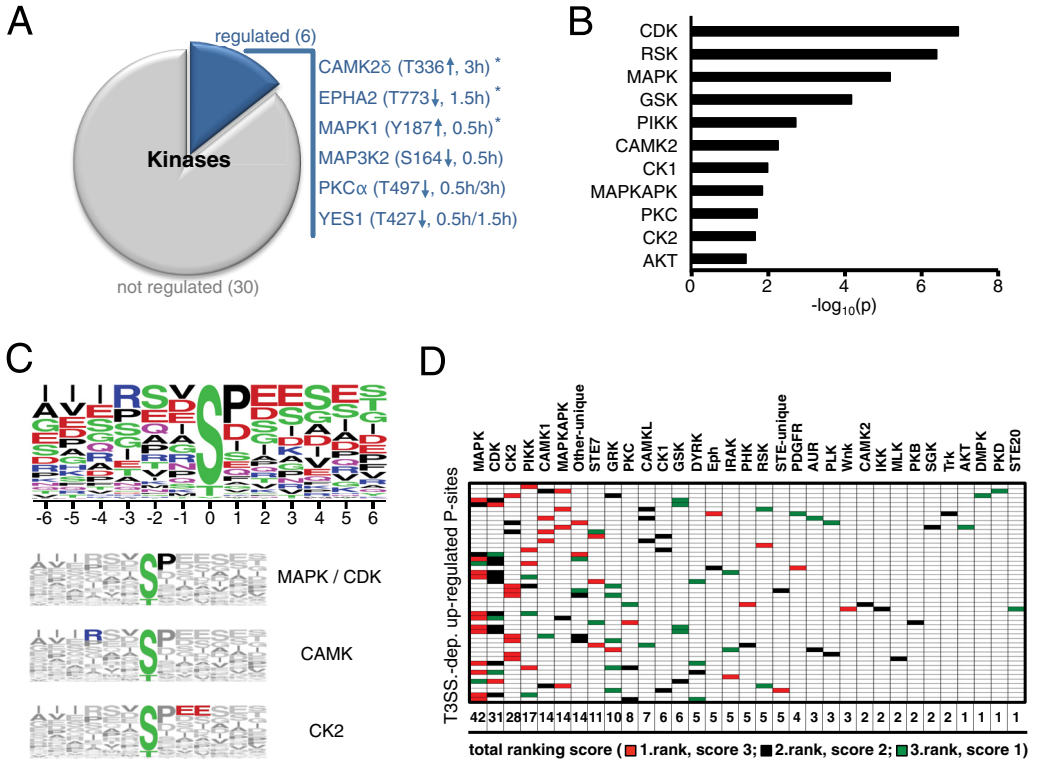

FIG. 3. **Assessment of host kinases involved in HeLa phosphoproteome alterations.** *A,* Pie chart representation of regulated (in blue) and not regulated (in gray) kinases based on a total number of 36 kinases that were detected in the phosphoproteome analysis. All six kinases with regulated phosphosites were depicted in detail with respective phosphosites and time points of regulation in parenthesis. The asterisk indicates T3SS-regulated phosphosites (arrows indicate an increase or decrease of phosphorylation). All sites refer to the canonical sequence of the Swiss-Prot entry in UniProt. CAMK2D, EPHA2, MAP3K2, and YES1 are class II sites. *B*, Enrichment of protein kinase families for all EPEC-regulated HeLa phosphoproteins based on 67 phosphoproteins (from a total of 110) that were listed in a mammalian kinase-substrate database ($p < 0.05$) (32). *C*, Phosphorylation motif analysis of all T3SS-dependently and -independently upregulated class I phosphosites using WebLogo (33). The numbering indicates the amino acid position with respect to the phosphosite. Identified kinase-specific consensus sequences were extracted and depicted in color on gray background (smaller panels). *D*, Kinase families were predicted for all 48 T3SS-dependently upregulated class I phosphosites using the phosphosite-specific prediction software GPS (34). If applicable, the top three predicted kinase families with the highest GPS score for each phosphosite were ranked and illustrated (1. rank: highest GPS score, in red; 2. rank: 2. highest GPS score, in black; 3. rank: 3. highest GPS score, in green). Each rank was associated with a GPS-unrelated ranking score as depicted in parenthesis. The summary of all ranking scores for each kinase family is illustrated at the bottom with top-ranking kinase families to low-ranking kinase families arranged from left to right.

MAPK1 (ERK2) activity is regulated by the phosphorylation of two residues within the activation loop: Thr-185 and Tyr-187 (47). Interestingly, a double-phosphorylated MAPK1 peptide harboring the phosphosite Tyr-187 and an undefined site was less abundant in EPEC Δ*escN*-infected cells when compared with uninfected cells at 0.5 hpi. In contrast, this decrease was not seen in EPEC WT-infected cells; instead a slight increase was observed when compared with uninfected cells early in infection. Although the second site was not localized, the results suggest that a functional T3SS triggers phosphorylation of Tyr-187. This corroborates previous studies that describe that T3SS-dependent activation of ERK1/2 pathways in epithelial host cells peaks early during EPEC infection (16, 48).

The identification of changes within multiple kinases and phosphorylation sites prompted us to assess the kinases most likely to be responsible for the observed regulations within EPEC-infection. Using complementary kinase enrichment analysis (32), kinases with an observed regulated phosphosite, such as MAPK1 ($p = 0.0000067$), CAMK2 ($p = 0.0056$), and PKC ($p = 0.02$), were significantly enriched. In addition to these kinases the CDK, RSK, GSK, PIKK, CK1, and CK2 families were also enriched within the regulated phosphoproteome (Fig. 3*B*), indicating that widespread changes in the kinome regulation occur in response to EPEC infection.

To further focus on the affected phosphosites and the host kinases directly responsible for these phosphorylation events during EPEC infection, we identified consensus kinase phosphorylation motifs among phosphosites that were upregulated both in a T3SS-dependent and -independent manner (Fig. 3*C*). Motif-based analysis extracted common MAPK and CDK (-S/T-P-), CAMK (-R-X-X-S/T-), and CK2 (-S/T-X-E-E-) consensus phosphorylation sequences. In addition, we pre-

dicted kinase families that may regulate each effector-dependent regulated phosphosite that showed increased abundance. These predictions were ranked according to their prediction score and a separate ranking associated score was assigned (Fig. 3*D*). In agreement with the complementary kinase enrichment analysis, the MAPK (score 42), CDK (score 31), CK2 (score 28), PIKK (score 17), CAMK1 (score 14), and MAPKAPK (score 14) kinase families were all identified as associated with T3SS-dependent regulation. In addition to these kinase families, we noted other kinases that were also repeatedly identified within the bioinformatic assessments of phosphorylation regulation. These included RSK, GSK, PKC, Eph receptor tyrosine kinase, and CAMK2, suggesting that these kinases may also play a role in regulating phosphorylation during EPEC-infection. In summary, the kinase-oriented bioinformatic analysis of the phosphoproteomic data suggests that several kinase families including CDK, CAMK2, PKC, CK2, and Eph represent signaling hubs during EPEC infection, with MAPK being the most prominent regulator.

EPEC Modulates Host-signaling Pathways during Infection—We next focused on defining host-signaling pathways that were affected by EPEC-mediated alterations in the phosphoproteome of HeLa epithelial cells. A network representation of all regulated phosphoproteins was generated by STRING, which revealed a complex, interconnected core set of 55 proteins that were functionally associated with each other (Fig. 4*A*). Consistent with our previous results, MAPK1 with its 14 connections represented a highly interconnected central node within the network (average number of connections per node = 2.8, S.D. = 2.7). The STRING software allows for an unbiased, automated addition of proteins (white nodes) that were functionally connected with but not part of the regulated phosphoproteome. We used this function to identify host proteins that might have been missed by the phosphoproteome analysis but are potentially targeted by EPEC and functional clusters that represent important signaling hubs during infection. Among these, epidermal growth factor receptor (EGFR) showed a multitude of functional associations. The autophosphorylation and transactivation of EGFR are known to occur during EPEC infection (49) supporting the inclusion of this node within the STRING network. Although not directly resolved in our phosphoproteomic screen, probably because of its membrane association, the STRING bioinformatic analysis confirmed that EGFR is an important signaling molecule during EPEC infection. Proteins that were T3SS-regulated and functionally associated with EGFR included the EGFR downstream effector MAPK1, EPHA2, and SH3 domain-containing kinase-binding protein 1 (SH3KBP1), also known as Cbl-interacting protein of 85 kDa (CIN85). Besides EGFR, receptor-interacting serine/threonine-protein kinase 1 (RIPK1), tumor necrosis factor receptor superfamily member 1A and B (TNFRSF1A/B), and tumor necrosis factor receptor type 1-associated DEATH domain protein (TRADD) also clustered together with sequestosome-1 (SQSTM1), TNF receptor-associated factor 2 and 4 (TRAF2/4), implicating EPEC effector-induced regulation of phosphorylation in host cell survival and innate immune pathways.

To further characterize the changes observed within the phosphoproteome, we performed a comprehensive pathway enrichment and functional annotation analysis using the following annotation categories: Swiss-Prot and Protein Information Resource keywords (SP_PIR_KEYWORD), Gene Ontology Biological Process Functional Annotation Tool (GOTERM_BP_FAT), Cellular Component Functional Annotation Tool (GOTERM_CC_FAT), BioCarta, and Kyoto Encyclopedia of Genes and Genomes (KEGG) pathway (36, 37). Enriched pathways, biological functions, and subcellular localizations ($p < 0.01$) that were unique to either T3SS- or non-T3SS-regulated phosphoproteins are shown in Fig. 4*B* (redundant annotation categories are illustrated in supplemental Fig. S3). The vast majority of enriched pathways that were specifically T3SS-independent comprise cellular processes within the nucleus, including RNA and DNA processing and organization. In contrast, all terms enriched for T3SS-regulated targets comprise other cellular processes, including immune signaling, intracellular trafficking, and cellular compartments such as the cytoskeleton and the nucleolus, that are known targets for EPEC T3SS effector-mediated subversion of host cell signaling (5). Consistent with the above-mentioned absence of membrane-associated EGFR and activated PKCα in the data set, the enrichment analysis of the whole regulated phosphoproteome revealed that the majority of observed phosphorylation events were cytoplasmic in nature ($p = 0.000071$).

An array of effectors orchestrates the modulation of host cell survival and immune responses during EPEC infection (reviewed in (5)). Within this screen several T3SS-regulated host proteins that are known to be involved in such processes were detected, including cytosolic phospholipase A2, the TNF receptor-associated factors TRAF2 and TRAF4 as well as EPHA2 (Table I) (50–53). The temporal phosphorylation pattern observed in EPHA2 was mirrored by CIN85 (SH3KBP1) and the Src kinase family protein groups (supplemental Fig. S4). Consistent with this similarity in the temporal phosphorylation patterns CIN85, via its interaction with c-Cbl, and SRC are associated with EPHA2 signaling (54–56) supporting the modulation of EPHA2 signaling in response to EPEC.

Recent findings suggest that effector-mediated targeting of cellular trafficking processes play an important role in EPEC pathogenesis (reviewed in (57)). However, many host components involved in pathogen manipulation of trafficking still remain to be defined. We identified several T3SS-regulated phosphoproteins in an array of host components involved in trafficking, such as synaptosomal-associated protein 23 (SNAP23), charged multivesicular body protein 7 (CHMP7), tumor protein D52 (TPD52), clathrin light chain A (CLTA), and rabphilin-11 (WDR44) (58–62). Others, such as Cdc42-inter-

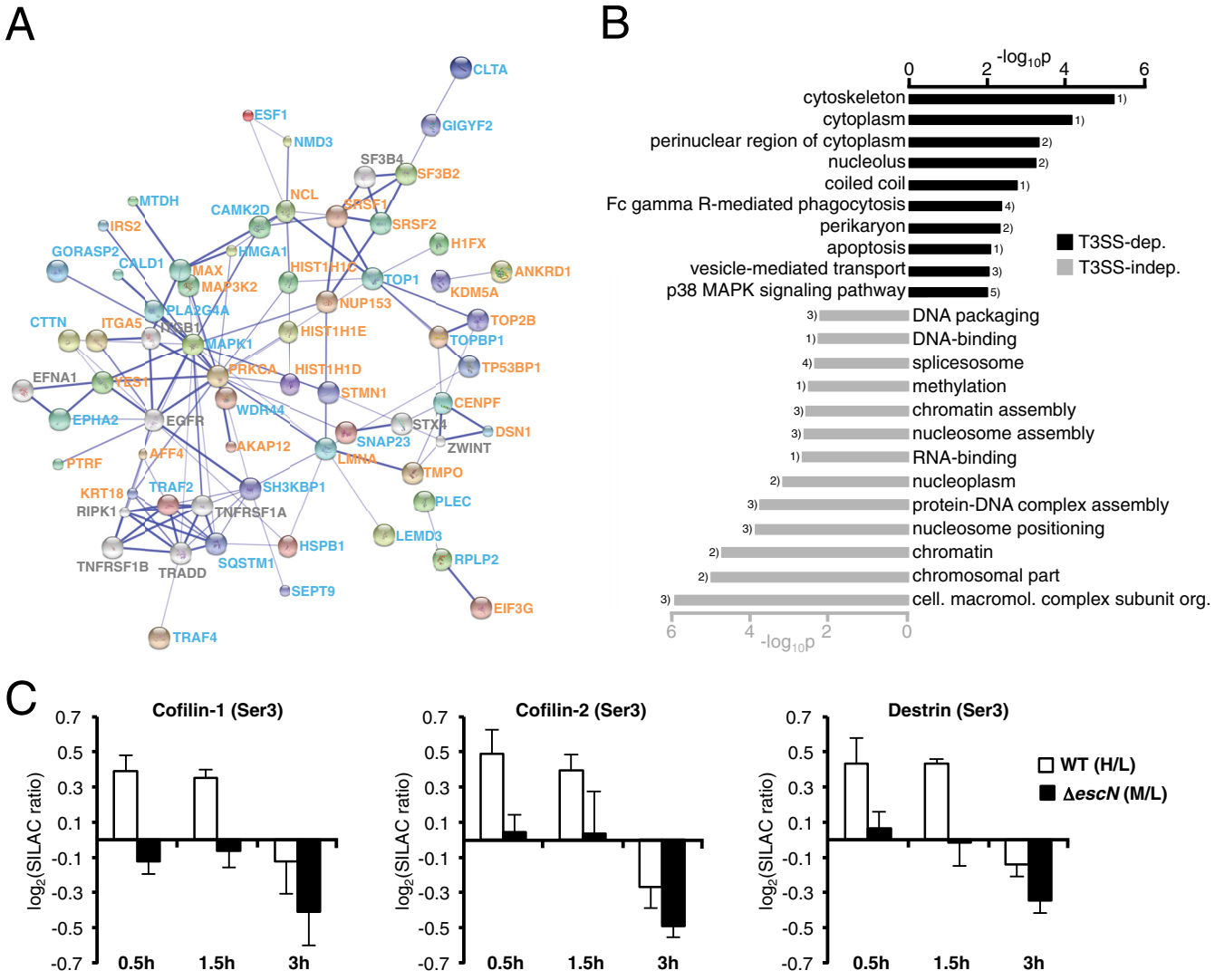

FIG. 4. **EPEC T3SS-dependent and -independent modulation of host cellular processes.** *A*, Graphical illustration of the functional association between all regulated phosphoproteins using STRING (medium confidence score) (35). The thicker the connecting line, the higher the confidence of the functional association between two proteins. Small nodes represent proteins were no structural information was available. Orange identifier: EPEC T3SS-independently regulated phosphoproteins; blue identifier: EPEC T3SS-dependently regulated phosphoproteins; gray identifier: 10 proteins that were automatically added by the STRING software to identify additional signaling hubs that are potentially involved in EPEC pathogenesis but were not identified in our phosphoproteome analysis. All node colors were automatically assigned by the STRING software. Only proteins with at least one connection are illustrated. *B*, Gene enrichment analysis of regulated phosphoproteins was performed using DAVID (36, 37). Following annotation categories were included and are indicated by number 1–5: SP_PIR_KEYWORD (1), GOTERM_CC_FAT (2), GOTERM_BP_FAT (3), KEGG pathway (4) and BioCarta (5). Only enriched cellular processes and biological functions that were unique to either T3SS-dependently regulated (black bars) or T3SS-independently regulated (gray bars) phosphoproteins were illustrated ($p < 0.01$). Additional annotations that were uniquely enriched, but very similar to the here shown categories were not included in this illustration. For assignments that were enriched for both T3SS-dependently and -independently regulated phosphoproteins see supplemental Fig. S3. *C*, Temporal resolution of the regulation of cofilin-1, cofilin-2, and destrin phosphorylation at Ser-3 as observed in the global HeLa cell phosphoproteome analysis. The average $\log_2$-transformed SILAC ratios for each phosphopeptide at 0.5, 1.5, and 3 hpi were plotted ($n = 3$; +S.D.). In white: EPEC WT-infected cells compared with uninfected control; in black: EPEC Δ*escN*-infected cells compared with uninfected control.

acting protein 4 (CIP4), MARCKS-related protein (MARCKSL1), and the multifunctional CIN85 (see above), have been implicated both in trafficking and cytoskeletal organization, two closely linked processes (63–66).

Host cytoskeletal rearrangement, especially during pedestal formation, is a major feature of EPEC pathogenesis (reviewed in (8)), which was also reflected by the identification of numerous cytoskeletal regulators in the screen. Cofilin (CFL1, CFL2), actin-depolymerizing factor (ADF, Destrin), and the Src substrate cortactin (CTTN) are well-characterized modulators of actin-dynamics within pedestals and were regulated at functional relevant phosphosites (Table I, Fig. 4*C*) (12, 67, 68).

Both CFL1 and ADF did not meet the 1.5-fold change in phosphorylation criteria; however, both showed a trend in persistent up-regulation in Ser-3 phosphorylation at 0.5 and 1.5 hpi, time points where pedestals are formed. In addition, we identified an array of novel players in cytoskeletal organization during EPEC pathogenesis including centrosomal protein of 170 kDa (CEP170), plectin (PLEC), caldesmon (CALD1), heat shock protein 27 (HSP27) and microtubule-associated protein 1B (MAP1B). Among the most prominently T3SS-regulated proteins was the cytoskeletal component septin-9 (SEPT9), a member of the filament-forming GTP-binding septin family. The drastic increase of Ser-30 phosphorylation in EPEC WT-infected HeLa cells when compared with EPEC Δ*escN*-infected cells over the entire course of infection suggests a crucial role of SEPT9 phosphorylation during EPEC infection (see below).

Besides the targets with clearly defined cellular roles numerous host cell proteins with functions that are either undefined or difficult to assign to specific host cell processes displayed a T3SS-regulated phosphorylation profile. Examples include the LIM domain only protein 7 (LMO7), ataxin-2-like protein (ATXN2L), neuroblast differentiation-associated protein AHNAK (AHNAK), PAT1-like protein 1 (PATL1), pleckstrin homology domain-containing family G member 3 (PLEKHG3), and calpastatin (CAST). These emphasize capacity of EPEC to interfere with host cell signaling beyond our current understanding of EPEC pathogenesis.

EPEC and Shigella Modulate a Similar Subset of Host Phosphoproteins—To our knowledge, this study represents the first global analysis of host phosphoproteome alterations upon infection with an extracellular diarrheagenic bacterial pathogen. We compared our data with the recently published phosphoproteome analyses of HeLa cells infected with *Salmonella enterica* serovar *typhimurium* (*S. typhimurium*) or *Shigella flexneri* (*S. flexneri*) (supplemental Fig. S5 and supplemental Table S9) (19–21). Despite different pathogens and divergent experimental conditions, the comparison revealed phosphopeptides that were similarly regulated by EPEC, *Shigella* and *Salmonella*. We further focused the comparative analysis on *S. flexneri*, which like EPEC is a diarrheagenic *E. coli* pathotype (supplemental Table S10). Unlike EPEC, *S. flexneri* invades host cells. The comparative analysis revealed that 64% of phosphoproteins regulated by EPEC were also regulated during *Shigella* infection (Fig. 5*A*). This common pool includes both proteins with identical and different targeted phosphosites. Among the phosphoproteins that were only targeted by EPEC, 55% were T3SS-regulated, whereas 45% were non-T3SS-regulated. This indicates that EPEC exerts both T3SS effector-dependent and -independent effects on the host phosphoproteome different from those observed within *Shigella* infection, potentially accounting for the differences in infection strategy between both pathogens.

We then examined peptides with identical sequences that were regulated in both data sets (Fig. 5*B*). A total of 48 identical phosphosites were targeted by both EPEC and *Shigella*. Forty-four percent of these sites had a different regulation pattern, *e.g.* upregulated during EPEC infection but down-regulated during *Shigella* infection. The majority comprised EPEC T3SS-dependent sites, suggesting an effector-mediated adaptation to a divergent infection strategy. Twenty-seven phosphosites were similarly regulated during *Shigella* infection, with an almost equal share of EPEC T3SS-dependent and -independent regulation. Several of the effector-independent sites belonged to proteins involved in nucleic acid organization and processing (Fig. 5*C*). In contrast, multiple shared sites that were T3SS-regulated were associated with proteins that either colocalize with the host cell cytoskeleton or are known cytoskeletal regulators or components. One of the most prominently regulated phosphosites in our screen, Ser-30 of SEPT9, was also regulated in *Shigella*-infected cells. Phosphorylation of Ser-30 was not only increased during EPEC and *Shigella* infection, but was also found to be similarly targeted in HeLa cells infected with *Salmonella*, another Gram-negative, invasive pathogen with functional T3SS machinery (20).

SEPT9 is a Novel Host Player in EPEC Pathogenesis—One of the most prominent events identified in this study was the T3SS-regulated, increased phosphorylation of SEPT9 during EPEC infection (Fig. 6*A*). Two independent proteomic screens previously identified a similar regulation of host SEPT9 phosphorylation during *Salmonella* and *Shigella* infection (19, 20). Moreover, earlier work has shown that SEPT9 is recruited to the actin-enriched site of bacterial host cell entry during *Listeria* and *Shigella* infection (69, 70). The role of SEPT9 in bacterial entry of the host cell and the molecular mechanisms underlying this process remain unclear. Although EPEC is a noninvasive pathogen lacking the intracellular lifestyle of *Listeria*, *Shigella*, and *Salmonella*, the intimate attachment to the host cell surface and the subsequent actin-driven pedestal formation require extensive cytoskeletal rearrangements similar to those used for engulfment of invasive bacteria. Thus, we hypothesized that SEPT9 and its phosphorylation at Ser-30 may play a critical role during EPEC pathogenesis, potentially as a regulator of EPEC attachment.

In humans SEPT9 belongs to a family of 13 septins (SEPT1–SEPT12 and SEPT14), that are GTP-binding proteins forming hetero-oligomeric complexes and higher-order structures such as filaments, rings and cages (reviewed in (71)). Alternative transcription initiation and splicing result in 18 different SEPT9 transcripts encoding 15 different isoforms, of which six have been confirmed at protein level (72, 73). The confirmed protein isoforms a–f (transcript variants v1–v4, v5/6, v7) share a C-terminal GTP-binding domain, preceded by a polybasic motif and an N-terminal region of variable length (Fig. 6*B*). N-terminal protein sequence alignment of SEPT9 isoforms a–f showed that the phosphopeptide identified in this study harboring the phosphorylated serine residue is only present in isoforms a–c and absent in isoforms d–f (Fig. 6*C*).

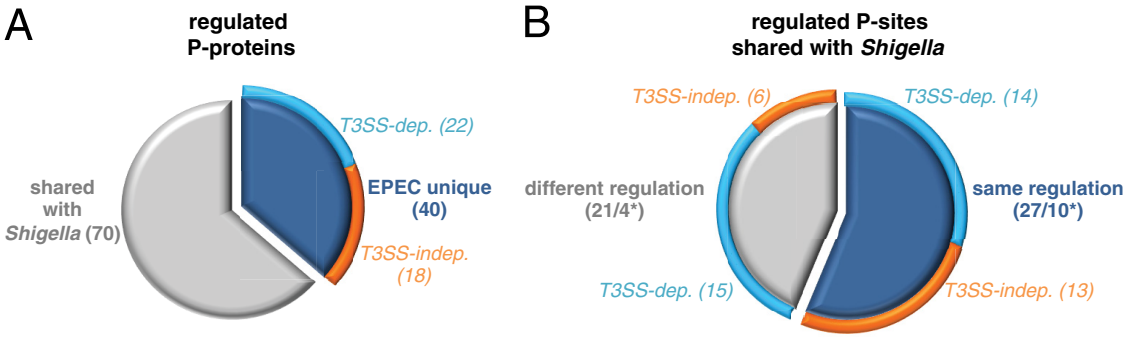

C

P-sites similarly regulated by EPEC and *Shigella*

UniProt ID	Protein name (Gene)	Regulated P-site	Protein funtion
Q9C0C2	182 kDa tankyrase-1-binding protein (TNKS1BP1)	S836 ↑	Unknown / Actin colocalization
Q96B97	Cbl-interacting protein of 85 kDa (CIN85)	S230 ↓	Cytoskeleton / Cell survival / Trafficking
P04792	Heat shock protein 27 (HSP27)	S82 ↑	Cytoskeleton
Q7Z417	Nuclear fragile X mental retardation-interacting protein 2 (NUFIP2)	S652 ↑	Unknown
Q9UHD8	Septin-9 (SEPT9)	S30 ↑	Cytoskeleton
P78344	Eukaryotic translation initiation factor 4 gamma 2 (EIF4G2)	T508 ↓	RNA translation
P10412	Histone H1.4 (HIST1H1E)	T18 ↓	DNA organization
P02545	Lamin-A/C (LMNA)	S22 ↓	Nucleus/DNA organization
P18615	Negative elongation factor E (NELFE)	S115 ↑	RNA processing
Q09666	Neuroblast differentiation-associated protein AHNAK (AHNAK)	S5830 ↑	Signaling

FIG. 5. ***Shigella versus* EPEC: Comparison of host phosphoproteomes.** Comparison of the EPEC-infected host phosphoproteome analysis with a previously published host phosphoproteome from *S. flexneri*-infected HeLa cells (19). *A*, All 110 regulated phosphoproteins from EPEC-infected HeLa cells were compared with phosphoproteins that showed at least a 1.5-fold change in phosphorylation in *S. flexneri*-infected HeLa cells. In gray: phosphoproteins that are regulated both in EPEC and *S. flexneri*-infected cells; in dark blue: phosphoproteins that were only regulated in EPEC-infected cells; in orange: EPEC T3SS-independently regulated phosphoproteins; in light blue: EPEC T3SS-dependently regulated phosphoproteins. The number of phosphoproteins in each category is depicted in parenthesis. *B*, Comparison of 48 class I phosphosites that were both regulated in EPEC- and *S. flexneri*-infected cells. In gray: phosphosites that showed a different regulation in EPEC-infected cells when compared with *S. flexneri*-infected cells; in dark blue: phosphosites that showed the same regulation in EPEC-infected cells when compared with *S. flexneri*-infected cells; in orange and light blue: as in *A*. The number of phosphoproteins in each category is depicted in parenthesis (asterisk: included number of phosphopeptides that carried, besides the common phosphosite, additional phosphosite(s) in either EPEC- or *S. flexneri*-infected cells and are thus not 100% identical). *C*, Phosphosites that were similarly regulated in EPEC- and *S. flexneri*-infected HeLa cells. The respective phosphoproteins were grouped according to T3SS-dependent (in blue) and -independent (in orange) regulation. Arrows indicate an increase or decrease of phosphorylation at the depicted sites.

The respective phosphosite corresponds to Ser-30 in isoform a, Ser-23 in isoform b and Ser-12 in isoform c.

The whole proteome analysis revealed that protein abundance of SEPT9 remained relatively consistent during infection with EPEC WT or mutant across all observed time points (supplemental Fig. S2*B*). This suggests that increased SEPT9 phosphorylation is not triggered by changes in SEPT9 expression levels, but solely because of changes at the post-translational level. This is supported by evidence from earlier work comparing the proteomes of EPEC WT- and Δ*escN*-infected polarized Caco-2 intestinal epithelial cells showing no significant changes in protein abundance of SEPT9 during infection (74). To further assess this observation, we performed real-time PCR using a primer pair that targeted all transcript variants v1–3 (isoforms a–c) of SEPT9 simultaneously. Also no significant changes in SEPT9 expression levels could be detected either in EPEC WT- or Δ*escN*-infected HeLa cells when compared with the uninfected control (Fig. 6*D*, left panel). Nevertheless, to ensure that the observed result was not because of the up-regulation of one isoform and down-regulation of another with no overall change in SEPT9 expression, we repeated the real-time PCR with primer pairs specific for each transcript variant. Analogous to previous results, the expression of each transcript variant remained unaltered during EPEC infection, indicating that the observed increased phosphorylation event was solely regulated at the post-translational level (Fig. 6*D*). The abundance of SEPT9 v2 transcripts was considerably lower than v1 and v3 in HeLa cells, as SEPT9 variants v2 remained undetected using a different variant-specific set of primers (data not shown). This suggests that SEPT9(a) and SEPT9(c) represent the predominant SEPT9 isoforms in HeLa cells.

Next we assessed the impact of SEPT9a/c on EPEC interactions with HeLa cells. SEPT9 knockdown by siRNA in HeLa cells successfully repressed the expression of isoforms a–c (Fig. 6*E*, left panel). Using this approach, we analyzed EPEC-mediated cytotoxicity as a measure of EPEC virulence. SEPT9 knockdown resulted in significantly reduced LDH-release and cell death of EPEC WT-infected HeLa cells compared with cells transfected with nontargeting control siRNA (Fig. 6*E*,

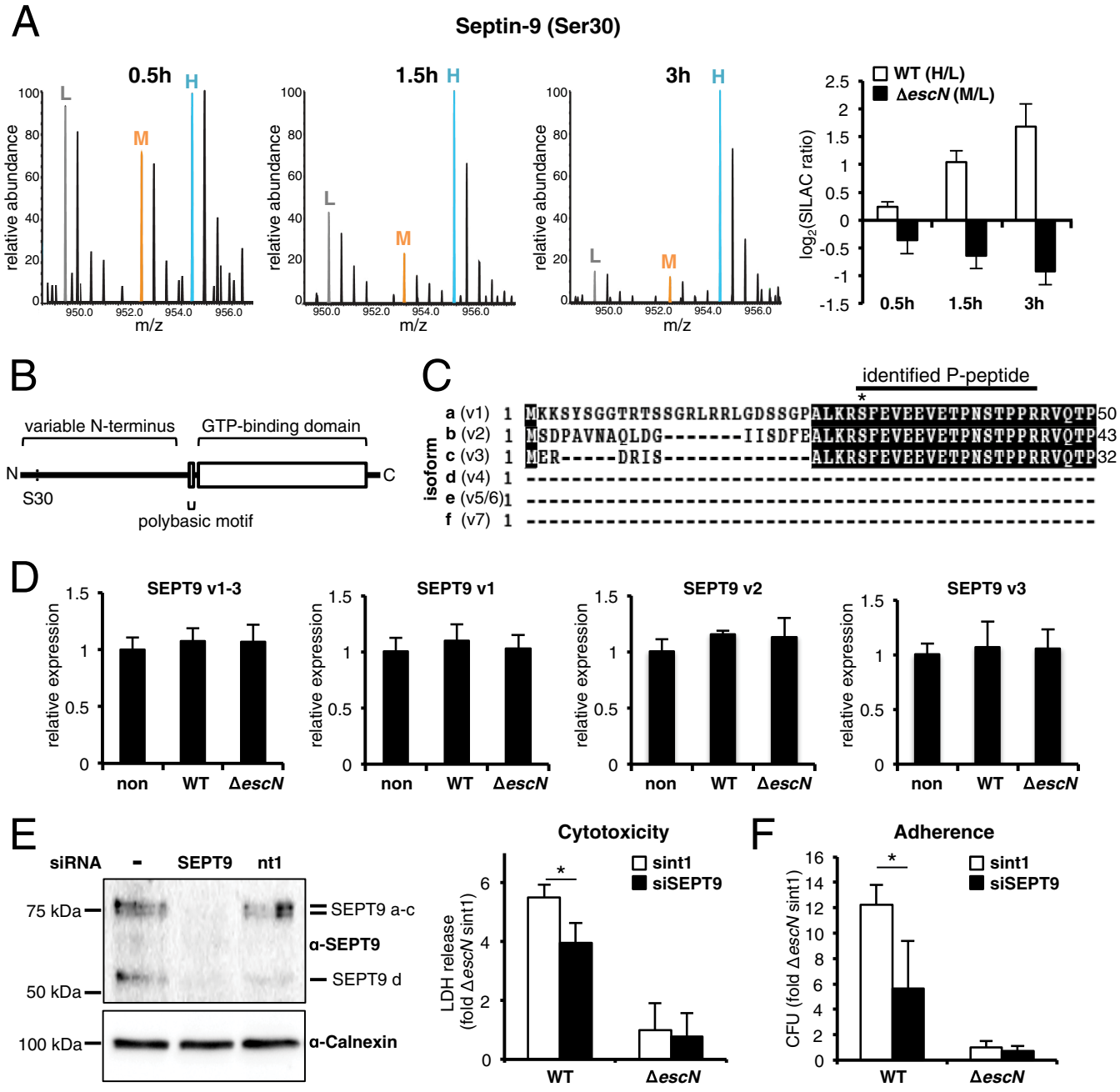

FIG. 6. **SEPT9 is relevant for EPEC virulence.** *A*, *left three panels*, Representative mass spectra of the phosphopeptide harboring the regulated SEPT9 Ser-30 phosphosite at 0.5, 1.5, and 3 hpi. The peaks at the m/z ratios corresponding to the respective SILAC labeled phosphopeptides are color-coded (gray: light label L; orange: medium label M; blue: heavy label H). *Right panel*, Regulation of SEPT9 Ser-30 phosphorylation as observed in the global HeLa cell phosphoproteome analysis. The average $\log_2$-transformed SILAC ratios for the corresponding phosphopeptide at 0.5, 1.5, and 3 hpi were plotted ($n = 3$; +S.D.). In white: EPEC WT-infected cells compared with uninfected control; in black: EPEC Δ*escN*-infected cells compared with uninfected control. *B*, Schematic illustration of SEPT9 domain structure including the approximate localization of the Ser-30 phosphosite. *C*. Protein sequence alignment of the N terminus of all experimentally confirmed SEPT9 protein isoforms a–f. The corresponding transcript variant nomenclature is depicted in parenthesis. Identical residues are shaded in black. The localization of the phosphopeptide (P-peptide), which was identified in the global phosphoproteome analysis, is indicated. The asterisk marks the position of the regulated serine phosphosite. *D*, SEPT9 expression control by real-time PCR analysis using primer pairs that targeted SEPT9 transcript variants v1–3, v1, v2, or v3. Original RNA was isolated from HeLa cells that were uninfected, EPEC WT- (WT) or EPEC Δ*escN*-infected (Δ*escN*) at 2 hpi. Expression levels were normalized relative to the average of expression in uninfected HeLa cells. The experiments were performed in three technical and three biological replicates ($n = 3$; +S.D.). *E*, *left panel*, Western blot analysis of SEPT9 siRNA knockdown in HeLa cells. Cells were either not transfected (−) or transfected with siRNA targeting SEPT9 or a nontargeting siRNA (nt1) as a control. Forty-eight hour post-transfection, cells were lysed and 15 μg of HeLa cell lysate was subjected to 12% SDS-PAGE and subsequent Western

right panel). No significant difference was observed for EPEC Δ*escN*-infected cells, thus confirming our finding that EPEC-mediated targeting of SEPT9 was T3SS-regulated (Fig. 6*E*, right panel). We then tested whether the observed impact on host cell death is because of SEPT9 regulation of EPEC adherence to the host cell surface. Knockdown of SEPT9 resulted in a significant decrease of EPEC WT adherence to HeLa cells (Fig. 6*F*). Consistent with the cytotoxicity results, no significant changes in the number of adherent bacteria were observed for EPEC Δ*escN*-infected cells during SEPT9 knockdown. These data strongly indicate that SEPT9 plays an important role in EPEC-host cell interactions and that SEPT9 is involved in T3SS-mediated EPEC adherence to the host cell surface.

We then assessed whether the T3SS-mediated phosphorylation event in the N-terminal SEPT9 serine residue is responsible for SEPT9 involvement in EPEC virulence. We used site-directed mutagenesis to generate FLAG-tagged SEPT9(a) constructs that carried a replacement of Ser-30 by either alanine to prevent phosphorylation (FLAG-SEPT9-S30A) or glutamate to mimic constitutive phosphorylation (FLAG-SEPT9-S30E). The transfection conditions used for subsequent experiments were chosen based on an earlier study to ensure low expression and thus allow for functional integrity and biological relevance of the transiently expressed FLAG-tagged SEPT9 constructs ((38), Experimental Procedures). Western blot analysis of HeLa cells transfected with respective constructs confirmed that both mutants and wild-type (FLAG-SEPT9-WT) expressed similar levels of FLAG-tagged SEPT9 (FLAG-SEPT9), indicating that neither Ser-30 substitutions had a negative impact on protein stability (Fig. 7*A*). To assess whether SEPT9 phosphorylation affects EPEC adherence, we transfected HeLa cells with wild-type or mutant SEPT9 constructs. When HeLa cells were transfected with FLAG-SEPT9-S30A, EPEC WT adherence was significantly decreased when compared with FLAG-SEPT9-WT transfected HeLa cells (Fig. 7*B*). However, when cells were transfected with FLAG-SEPT9-S30E, EPEC WT adherence was similar to cells transfected with FLAG-SEPT9-WT. EPEC Δ*escN*-infected HeLa cells showed no significant difference in bacterial adherence. These data not only revealed that blocking Ser-30 phosphorylation impairs EPEC WT adherence but also that phosphorylation mimicking by glutamate leads to a functional rescue and promotes EPEC WT adherence to the host cell.

Adherence to host cells is a key strategy of EPEC virulence and is functionally connected with EPEC-induced host cell death in cell culture models. Thus, assessment of cell death by LDH-release analysis was used as an independent approach to confirm the previous findings. When compared with FLAG-SEPT9-WT transfected cells, HeLa cells transfected with FLAG-SEPT9-S30A and infected with EPEC WT displayed less cytotoxicity (Fig. 7*C*, $p = 0.067$). In contrast, cells transfected with FLAG-SEPT9-S30E and infected with EPEC WT showed a significant increase in LDH-release when compared with FLAG-SEPT9-S30A transfected and EPEC WT-infected cells. This again confirms the functional rescue by the phospho-mimicking mutant and underlines the critical role of SEPT9 phosphorylation in EPEC interactions with host cells. As before, no significant differences were noted in EPEC Δ*escN*-infected cells.

Collectively, these SEPT9 studies validate and functionally characterize the phosphoproteomic data. These results suggest that SEPT9 is a novel key host player in EPEC pathogenesis controlling the pathogen's attachment to the host cell surface. Furthermore, T3SS-mediated phosphorylation of Ser-30 in SEPT9 is critical for efficient bacterial adherence.

DISCUSSION

Alterations in host protein phosphorylation following infection can provide substantial insight into the molecular mechanisms by which human pathogens exploit host cell signaling to cause disease. Here we present the first study that examines the global impact of an extracellular diarrheagenic bacterial pathogen on the host phosphoproteome.

The infection strategies of invasive and extracellular pathogens differ significantly. Because EPEC remains at the host cell surface and does not replicate inside the host cell, it experiences a reduced host exposure when compared with *Salmonella* and *Shigella*. In addition, EPEC encodes a more limited T3SS effector repertoire: *e.g.* it lacks a phosphothreonine lyase such as the *Salmonella* effector SpvC or the *Shigella* effector OspF (75, 76). This lack of effectors, especially those with a significant role in host phosphoproteome modulation, and the limited host exposure suggests that EPEC might have a reduced impact on the host phosphoproteome.

blotting using an antiSEPT9 antibody (39) and an anticalnexin antibody as a total protein control. Expected SEPT9 isoforms are indicated on the right. *Right panel*, LDH-release assay of siRNA transfected and EPEC WT- or Δ*escN*-infected HeLa cells to measure the impact of SEPT9 on EPEC-mediated cytotoxicity and thus virulence. HeLa cells were transfected with siRNA targeting SEPT9 (siSEPT9, in black) or a nontargeting siRNA (sint1, in white). Forty-eight hour post-transfection, cells were infected for 3 h, LDH-release was determined and normalized relative to the average of LDH-release from EPEC Δ*escN*-infected and nontargeting siRNA-transfected HeLa cells ($n = 3$; +S.D.; *, $p < 0.05$). *F*, Cell adherence assay of siRNA transfected and EPEC WT- or Δ*escN*-infected HeLa cells to determine the role of SEPT9 in bacterial adherence to the host cell surface. HeLa cells were transfected with siRNA as in *E*. Forty-eight hour post-transfection, cells were infected for 2 h, washed eight times with PBS+/+ and cfu counts were determined as a measure of bacterial adherence. The cfu counts were normalized relative to the average cfu count that was determined from EPEC Δ*escN*-infected and nontargeting siRNA-transfected HeLa cells ($n = 3$; +S.D.; *, $p < 0.05$).

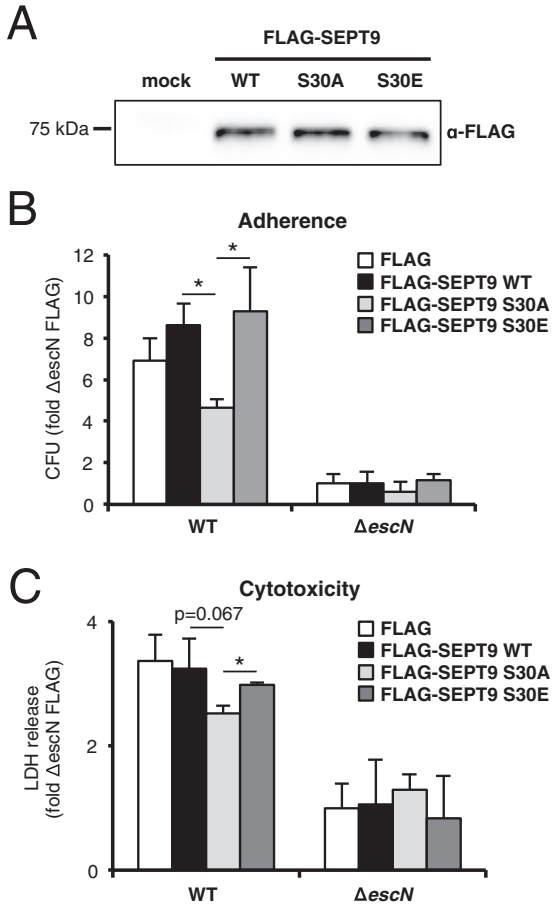

FIG. 7. **Role of SEPT9 phosphorylation in EPEC pathogenesis.** *A*, Expression test. Western blot analysis of HeLa cells that were transfected with N-terminally FLAG-tagged SEPT9 constructs including wild-type (WT) and mutant SEPT9 constructs that carried a replacement of Ser-30 with either alanine (S30A) or glutamate (S30E). Twenty-four hour post-transfection, 13 μg of HeLa cell lysate was separated using 12% SDS-PAGE and subsequently probed with an antiFLAG M2 antibody (mock, empty vector-transfected control). *B*, Cell adherence assay of FLAG-SEPT9 construct-transfected and EPEC WT- or Δ*escN*-infected HeLa cells to determine the role of SEPT9 phosphorylation in bacterial adherence. HeLa cells were transfected with plasmids encoding the proteins that are indicated in the legend. Twenty-four hour post-transfection, cells were infected for 2 h, washed eight times with PBS+/+, and cfu counts were determined. The cfu counts were normalized relative to the average cfu count deriving from EPEC Δ*escN*-infected and empty FLAG-vector control-transfected HeLa cells ($n = 3$; +S.D.; *, $p < 0.05$). *C*, LDH-release assay to analyze the impact of SEPT9 Ser-30 phosphorylation on EPEC-mediated cytotoxicity. The experiment was performed similar as in *B*, except that 3 hpi LDH-release was determined and normalized relative to the average LDH-release from EPECΔ*escN*-infected and empty FLAG-vector control-transfected HeLa cells ($n = 3$; +S.D.; *, $p < 0.05$).

Consistent with this hypothesis we observed a less profound impact on the host phosphoproteome by EPEC compared with earlier phosphoproteomic profiling studies of *Shigella* or *Salmonella* (19, 20). Nevertheless, our unbiased and comprehensive phosphoproteome analysis revealed that EPEC still triggers extensive changes in the host phosphoproteome far beyond what was established from targeted protein studies.

We observed a time-dependent increase of regulated phosphosites, which correlated to increased pathogen exposure. As expected, the impact on host phosphorylation was more profound in EPEC WT-infected cells when compared with T3SS-deficient mutant-infected cells. The observed T3SS-dependent alterations mainly affected cellular components that are known targets of pathogens: *e.g.* MAPKs have been implicated as an important signaling hub during host infection with EPEC and various other bacterial pathogens, and are often targeted by translocated bacterial virulence factors (16, 48, 77–80). Based on kinase enrichment, motif and T3SS-regulated phosphosite analysis as well as the identification of a T3SS-regulated MAPK activation loop phosphopeptide, our results emphasize the central role of MAPK during EPEC infection. In general, the data suggest that EPEC T3S effectors modulate host signaling via phosphorylation of a wide range of cellular processes. Besides previously unrecognized host components in bacterial pathogenesis such as EPHA2 and TPD52, we also identified signaling hubs that are known targets for EPEC virulence, such as TRAF2 (81, 82), but that had not been shown to be impacted by phosphorylation upon EPEC infection.

EPEC-mediated host cytoskeletal reorganization is the best studied process in EPEC pathogenesis (8). However, the role of phosphorylation in this process is not well understood, and research thus far has mainly focused on Tyr-phosphorylation of the bacterial effector Tir and components of the classical NCK-N-WASP-ARP2/3 pathway (10, 12). The data presented here provide additional mechanistic insights into serine and threonine phosphorylation-mediated cytoskeletal regulation during EPEC infection. We observed that targets within the cytoskeleton were the cellular components most impacted by T3S effectors. Actin-depolymerization factor and cofilin had increased phosphorylation at Ser-3 early in infection. Cofilin is recruited to pedestals where it presumably modulates actin-filament dynamics (67). Ser-3 phosphorylation by LIMK has been shown to inhibit the actin-filament depolymerizing activity of cofilin suggesting a T3S-effector mediated stabilization of actin filaments via this pathway early during infection (68). An earlier model proposed that cofilin inactivation via the RhoA-ROCK pathway stabilizes the actin microfilaments in transient filopodia that form and disappear within 30 min of infection (83, 84). We observed an increased abundance of phosphorylated cofilin up to 1.5 h, which indicates an additional role beyond filopodia stabilization and possibly extends to actin filament stabilization within pedestals. Another regulator of actin filament dynamics, HSP27, showed increased phosphorylation at Ser-82 in a T3SS-dependent manner during EPEC infection. Phosphorylation of Ser-82, one of three sites targeted by MAPKAP2, promotes actin filament formation (85, 86). This indicates that, in addition to cofilin phosphorylation, HSP27 phosphorylation might also function as a

T3SS-triggered phosphorylation event that stabilizes actin filaments during EPEC infection.

In contrast to cofilin and HSP27 phosphorylation, the biological relevance and functional consequence of N-terminal SEPT9 Ser-30 phosphorylation was previously unknown. T3SS-dependent increase in SEPT9 phosphorylation was one of the most prominent events detected in this study. Using siRNA knockdown and phosphosite mutants we showed for the first time that SEPT9 and its phosphorylation play a critical role in EPEC pathogenesis by impacting on bacterial adherence to the host cell surface. SEPT9 is involved in a plethora of cellular processes including actin dynamics, microtubule regulation, cytokinesis, vesicle targeting, exocytosis, angiogenesis, cell proliferation, shape, and motility as well as bacterial autophagy. Its architecture differs from most other septins as it is missing a C-terminal coiled-coil domain (71). SEPT9 occupies the terminal position of octameric septin complexes (SEPT9-SEPT7-SEPT6-SEPT2-SEPT2-SEPT6-SEPT7-SEPT9), and can self-assemble via its N-terminal domain within the so-called NC-interface (interface of N- and C-terminal domains). It also regulates the formation of higher-order septin structures such as filaments and rings. Deletion of its N terminus blocks septin higher-order structure formation (38). The fact that the observed SEPT9 phosphorylation is localized within the N terminus indicates a possible function in higher-order septin structure assembly. In yeast, the terminal positions of septin octamers are occupied by Cdc11 or Shs1, which are phosphorylated and have a more extended C-terminal but shorter N-terminal domain than human SEPT9 (87). Shs1 is phosphorylated within its C terminus and phosphomimetic mutants of respective sites impact yeast septin higher-order structure organization (88). However, the role of phosphorylation in human SEPT9 regulation is not well understood. A functional consequence of SEPT9 phosphorylation was only recently reported: Cdk1-dependent phosphorylation of an N-terminal threonine residue promoted SEPT9 interaction with Pin1 protein to promote cytokinesis (89). Because septins are involved in actin dynamics and actin remodeling plays a critical role in EPEC pedestal formation and bacterial adherence, it is possible that the observed adherence phenotype is because of an altered interaction of septin with pedestal components. Among those components, CIN85 is a potential candidate. CIN85 regulates various cellular processes including the organization of filamentous actin (90), interacts with the SEPT9 N terminus (91) and was identified among the most prominent T3SS-regulated phosphoproteins in our analysis.

Our findings with SEPT9 may also apply to other bacterial pathogens. Recent studies documented SEPT9 recruitment to the site of *Listeria* and *Shigella* host cell entry and established a crucial role of septin in bacterial invasion (69, 70). In addition SEPT9 is recruited to ARP2/3- (for *Listeria*) and ARP2/3-N-WASP-based (for *Shigella*) actin-tails that cytosolic *Listeria* and *Shigella* use for intracellular motility. Moreover SEPT9 is essential for the entrapment of cytosolic *Shigella* in septin cages, which restrict the actin-based bacterial motility (92). Increased SEPT9 Ser-30 phosphorylation was also detected in recent phosphoproteomic studies of *Shigella*- and *Salmonella*-infected epithelial cells (19, 20), indicating a potential link between SEPT9 phosphorylation and the contribution of SEPT9 to the pathogenesis of *Shigella* and possible also of other bacterial pathogens, such as *Salmonella* and *Listeria*.

Collectively these data provide a dynamic landscape of EPEC-mediated alterations within the host phosphoproteome. We identified SEPT9 as a novel host target in EPEC pathogenesis, established the biological relevance of SEPT9 Ser-30 phosphorylation, and provide mechanistic insights into EPEC's strategy to hijack host signaling.

Acknowledgments—We thank Nikolay Stoynov for technical assistance with the mass spectrometry and Wanyin Deng and Natalie Marshall for critical reading of the manuscript. LJF is the Canada Research Chair in Quantitative Proteomics. The mass spectrometry infrastructure used in this work was supported by the Canada Foundation for Innovation, the British Columbia (BC) Knowledge Development Fund and the BC Proteomics Network.

* This work was supported by Canadian Institutes of Health Research (CIHR) Operating Grants MOP-136976 (to B.B.F.), MOP-77688 (to L.J.F.) and MOP-133660 (to W.S.T.). RS and NES recipient of a Postdoctoral Trainee Award from the Michael Smith Foundation for Health Research (MSFHR). KI supported by the Japan Society for the Promotion of Science (JSPS) Postdoctoral Fellowship for Research Abroad. NES supported by a National Health and Medical Research Council of Australia (NHMRC) Overseas (Biomedical) Fellowship (APP1037373).

S This article contains supplemental Figs. S1 to S5 and Tables S1 to S10.

‡‡ To whom correspondence may be addressed: Michael Smith Laboratories, University of British Columbia, 301-2815 East Mall, Vancouver, British Columbia V6T 1Z4, Canada. Tel.: +1-604-822-2210; Fax: +1-604-822-9830; E-mail: bfinlay@msl.ubc.ca; Centre for High-Throughput Biology and Department of Biochemistry and Molecular Biology, University of British Columbia, 2125 East Mall, Vancouver, BC V6T 1Z4, Canada. Tel.: +1-604-822-8311; Fax: +1-604-822-2114; E-mail: foster@chibi.ubc.ca.

REFERENCES

1. Croxen, M. A., Law, R. J., Scholz, R., Keeney, K. M., Wlodarska, M., and Finlay, B. B. (2013) Recent advances in understanding enteric pathogenic Escherichia coli. *Clin. Microbiol. Rev.* **26,** 822–880
2. Deng, W., Yu, H. B., de Hoog, C. L., Stoynov, N., Li, Y., Foster, L. J., and Finlay, B. B. (2012) Quantitative proteomic analysis of type III secretome of enteropathogenic Escherichia coli reveals an expanded effector repertoire for attaching/effacing bacterial pathogens. *Mol. Cell. Proteomics* **11,** 692–709
3. Iguchi, A., Thomson, N. R., Ogura, Y., Saunders, D., Ooka, T., Henderson, I. R., Harris, D., Asadulghani, M., Kurokawa, K., Dean, P., Kenny, B., Quail, M. A., Thurston, S., Dougan, G., Hayashi, T., Parkhill, J., and Frankel, G. (2009) Complete genome sequence and comparative genome analysis of enteropathogenic Escherichia coli O127:H6 strain E2348/69. *J. Bacteriol.* **191,** 347–354
4. Cornelis, G. R. (2006) The type III secretion injectisome. *Nat. Rev. Microbiol.* **4,** 811–825
5. Wong, A. R. C., Pearson, J. S., Bright, M. D., Munera, D., Robinson, K. S., Lee, S. F., Frankel, G., and Hartland, E. L. (2011) Enteropathogenic and enterohaemorrhagic Escherichia coli: even more subversive elements. *Mol. Microbiol.* **80,** 1420–1438

6. Kenny, B., DeVinney, R., Stein, M., Reinscheid, D. J., Frey, E. A., and Finlay, B. B. (1997) Enteropathogenic E. coli (EPEC) transfers its receptor for intimate adherence into mammalian cells. *Cell* **91,** 511–520
7. Mills, E., Baruch, K., Charpentier, X., Kobi, S., and Rosenshine, I. (2008) Real-time analysis of effector translocation by the type III secretion system of enteropathogenic Escherichia coli. *Cell Host Microbe* **3,** 104–113
8. Navarro-Garcia, F., Serapio-Palacios, A., Ugalde-Silva, P., Tapia-Pastrana, G., and Chavez-Dueñas, L. (2013) Actin cytoskeleton manipulation by effector proteins secreted by diarrheagenic Escherichia coli pathotypes. *BioMed. Res. Int.* 2013:374395
9. Ribet, D., and Cossart, P. (2010) Post-translational modifications in host cells during bacterial infection. *FEBS Lett.* **584,** 2748–2758
10. Gruenheid, S., DeVinney, R., Bladt, F., Goosney, D., Gelkop, S., Gish, G. D., Pawson, T., and Finlay, B. B. (2001) Enteropathogenic E. coli Tir binds Nck to initiate actin pedestal formation in host cells. *Nat. Cell Biol.* **3,** 856–859
11. Gao, X., Wan, F., Mateo, K., Callegari, E., Wang, D., Deng, W., Puente, J., Li, F., Chaussee, M. S., Finlay, B. B., Lenardo, M. J., and Hardwidge, P. R. (2009) Bacterial effector binding to ribosomal protein s3 subverts NF-kappaB function. *PLoS Pathog.* **5,** e1000708
12. Nieto-Pelegrin, E., and Martinez-Quiles, N. (2009) Distinct phosphorylation requirements regulate cortactin activation by TirEPEC and its binding to N-WASP. *Cell Commun. Signal. CCS* **7,** 11
13. Nieto-Pelegrin, E., Meiler, E., Martín-Villa, J. M., Benito-León, M., and Martinez-Quiles, N. (2014) Crk adaptors negatively regulate actin polymerization in pedestals formed by enteropathogenic Escherichia coli (EPEC) by binding to Tir effector. *PLoS Pathog.* **10,** e1004022
14. Shifrin, Y., Kirschner, J., Geiger, B., and Rosenshine, I. (2002) Enteropathogenic Escherichia coli induces modification of the focal adhesions of infected host cells. *Cell. Microbiol.* **4,** 235–243
15. Shames, S. R., Deng, W., Guttman, J. A., de Hoog, C. L., Li, Y., Hardwidge, P. R., Sham, H. P., Vallance, B. A., Foster, L. J., and Finlay, B. B. (2010) The pathogenic E. coli type III effector EspZ interacts with host CD98 and facilitates host cell prosurvival signaling. *Cell. Microbiol.* **12,** 1322–1339
16. De Grado, M., Rosenberger, C. M., Gauthier, A., Vallance, B. A., and Finlay, B. B. (2001) Enteropathogenic Escherichia coli infection induces expression of the early growth response factor by activating mitogen-activated protein kinase cascades in epithelial cells. *Infect. Immun.* **69,** 6217–6224
17. Kenny, B., and Finlay, B. B. (1997) Intimin-dependent binding of enteropathogenic Escherichia coli to host cells triggers novel signaling events, including tyrosine phosphorylation of phospholipase C-gamma1. *Infect. Immun.* **65,** 2528–2536
18. Goosney, D. L., Celli, J., Kenny, B., and Finlay, B. B. (1999) Enteropathogenic Escherichia coli inhibits phagocytosis. *Infect. Immun.* **67,** 490–495
19. Schmutz, C., Ahrné, E., Kasper, C. A., Tschon, T., Sorg, I., Dreier, R. F., Schmidt, A., and Arrieumerlou, C. (2013) Systems-level overview of host protein phosphorylation during Shigella flexneri infection revealed by phosphoproteomics. *Mol. Cell. Proteomics* **12,** 2952–2968
20. Rogers, L. D., Brown, N. F., Fang, Y., Pelech, S., and Foster, L. J. (2011) Phosphoproteomic analysis of Salmonella-infected cells identifies key kinase regulators and SopB-dependent host phosphorylation events. *Sci. Signal.* **4,** rs9
21. Imami, K., Bhavsar, A. P., Yu, H., Brown, N. F., Rogers, L. D., Finlay, B. B., and Foster, L. J. (2013) Global impact of Salmonella pathogenicity island 2-secreted effectors on the host phosphoproteome. *Mol. Cell. Proteomics* **12,** 1632–1643
22. Ong, S.-E., and Mann, M. (2006) A practical recipe for stable isotope labeling by amino acids in cell culture (SILAC). *Nat. Protoc.* **1,** 2650–2660
23. Levine, M. M., Bergquist, E. J., Nalin, D. R., Waterman, D. H., Hornick, R. B., Young, C. R., and Sotman, S. (1978) Escherichia coli strains that cause diarrhoea but do not produce heat-labile or heat-stable enterotoxins and are noninvasive. *Lancet* **1,** 1119–1122
24. Gauthier, A., Puente, J. L., and Finlay, B. B. (2003) Secretin of the enteropathogenic Escherichia coli type III secretion system requires components of the type III apparatus for assembly and localization. *Infect. Immun.* **71,** 3310–3319
25. Rappsilber, J., Mann, M., and Ishihama, Y. (2007) Protocol for micro-purification, enrichment, prefractionation and storage of peptides for proteomics using StageTips. *Nat. Protoc.* **2,** 1896–1906
26. Sugiyama, N., Masuda, T., Shinoda, K., Nakamura, A., Tomita, M., and Ishihama, Y. (2007) Phosphopeptide enrichment by aliphatic hydroxy acid-modified metal oxide chromatography for nano-LC-MS/MS in proteomics applications. *Mol. Cell. Proteomics* **6,** 1103–1109
27. Kyono, Y., Sugiyama, N., Imami, K., Tomita, M., and Ishihama, Y. (2008) Successive and selective release of phosphorylated peptides captured by hydroxy acid-modified metal oxide chromatography. *J. Proteome Res.* **7,** 4585–4593
28. Cox, J., and Mann, M. (2008) MaxQuant enables high peptide identification rates, individualized p.p.b.-range mass accuracies and proteome-wide protein quantification. *Nat. Biotechnol.* **26,** 1367–1372
29. Cox, J., Neuhauser, N., Michalski, A., Scheltema, R. A., Olsen, J. V., and Mann, M. (2011) Andromeda: a peptide search engine integrated into the MaxQuant environment. *J. Proteome Res.* **10,** 1794–1805
30. Olsen, J. V., Blagoev, B., Gnad, F., Macek, B., Kumar, C., Mortensen, P., and Mann, M. (2006) Global, *in vivo*, and site-specific phosphorylation dynamics in signaling networks. *Cell* **127,** 635–648
31. Saeed, A. I., Sharov, V., White, J., Li, J., Liang, W., Bhagabati, N., Braisted, J., Klapa, M., Currier, T., Thiagarajan, M., Sturn, A., Snuffin, M., Rezantsev, A., Popov, D., Ryltsov, A., Kostukovich, E., Borisovsky, I., Liu, Z., Vinsavich, A., Trush, V., and Quackenbush, J. (2003) TM4: a free, open-source system for microarray data management and analysis. *BioTechniques* **34,** 374–378
32. Lachmann, A., and Ma'ayan, A. (2009) KEA: kinase enrichment analysis. *Bioinforma. Oxf. Engl.* **25,** 684–686
33. Crooks, G. E., Hon, G., Chandonia, J.-M., and Brenner, S. E. (2004) WebLogo: a sequence logo generator. *Genome Res.* **14,** 1188–1190
34. Xue, Y., Liu, Z., Cao, J., Ma, Q., Gao, X., Wang, Q., Jin, C., Zhou, Y., Wen, L., and Ren, J. (2011) GPS 2.1: enhanced prediction of kinase-specific phosphorylation sites with an algorithm of motif length selection. *Protein Eng. Des. Sel. PEDS* **24,** 255–260
35. Jensen, L. J., Kuhn, M., Stark, M., Chaffron, S., Creevey, C., Muller, J., Doerks, T., Julien, P., Roth, A., Simonovic, M., Bork, P., and von Mering, C. (2009) STRING 8 – a global view on proteins and their functional interactions in 630 organisms. *Nucleic Acids Res.* **37,** D412–D416
36. Huang, D. W., Sherman, B. T., and Lempicki, R. A. (2009) Systematic and integrative analysis of large gene lists using DAVID bioinformatics resources. *Nat. Protoc.* **4,** 44–57
37. Huang, D. W., Sherman, B. T., and Lempicki, R. A. (2009) Bioinformatics enrichment tools: paths toward the comprehensive functional analysis of large gene lists. *Nucleic Acids Res.* **37,** 1–13
38. Kim, M. S., Froese, C. D., Estey, M. P., and Trimble, W. S. (2011) SEPT9 occupies the terminal positions in septin octamers and mediates polymerization-dependent functions in abscission. *J. Cell Biol.* **195,** 815–826
39. Surka, M. C., Tsang, C. W., and Trimble, W. S. (2002) The mammalian septin MSF localizes with microtubules and is required for completion of cytokinesis. *Mol. Biol. Cell* **13,** 3532–3545
40. Crane, J. K., Majumdar, S., and Pickhardt, D. F. (1999) Host cell death due to enteropathogenic Escherichia coli has features of apoptosis. *Infect. Immun.* **67,** 2575–2584
41. Law, R. J., Gur-Arie, L., Rosenshine, I., and Finlay, B. B. (2013) *In vitro* and *in vivo* model systems for studying enteropathogenic Escherichia coli infections. *Cold Spring Harb. Perspect. Med.* **3,** a009977
42. Mills, E., Baruch, K., Aviv, G., Nitzan, M., and Rosenshine, I. (2013) Dynamics of the type III secretion system activity of enteropathogenic Escherichia coli. *mBio* **4,** e00303–13
43. Shames, S. R., Bhavsar, A. P., Croxen, M. A., Law, R. J., Mak, S. H. C., Deng, W., Li, Y., Bidshari, R., de Hoog, C. L., Foster, L. J., and Finlay, B. B. (2011) The pathogenic Escherichia coli type III secreted protease NleC degrades the host acetyltransferase p300. *Cell. Microbiol.* **13,** 1542–1557
44. Ubersax, J. A., and Ferrell, J. E. (2007) Mechanisms of specificity in protein phosphorylation. *Nat. Rev. Mol. Cell Biol.* **8,** 530–541
45. Cazaubon, S., Bornancin, F., and Parker, P. J. (1994) Threonine-497 is a critical site for permissive activation of protein kinase C alpha. *Biochem. J.* **301,** 443–448
46. Crane, J. K., and Oh, J. S. (1997) Activation of host cell protein kinase C by enteropathogenic Escherichia coli. *Infect. Immun.* **65,** 3277–3285
47. Payne, D. M., Rossomando, A. J., Martino, P., Erickson, A. K., Her, J. H., Shabanowitz, J., Hunt, D. F., Weber, M. J., and Sturgill, T. W. (1991) Identification of the regulatory phosphorylation sites in pp42/mitogen-activated protein kinase (MAP kinase). *EMBO J.* **10,** 885–892

48. Savkovic, S. D., Ramaswamy, A., Koutsouris, A., and Hecht, G. (2001) EPEC-activated ERK1/2 participate in inflammatory response but not tight junction barrier disruption. *Am. J. Physiol. Gastrointest. Liver Physiol.* **281,** G890–G898
49. Roxas, J. L., Koutsouris, A., and Viswanathan, V. K. (2007) Enteropathogenic Escherichia coli-induced epidermal growth factor receptor activation contributes to physiological alterations in intestinal epithelial cells. *Infect. Immun.* **75,** 2316–2324
50. Linkous, A., and Yazlovitskaya, E. (2010) Cytosolic phospholipase A2 as a mediator of disease pathogenesis. *Cell. Microbiol.* **12,** 1369–1377
51. Miao, H., Burnett, E., Kinch, M., Simon, E., and Wang, B. (2000) Activation of EphA2 kinase suppresses integrin function and causes focal-adhesion-kinase dephosphorylation. *Nat. Cell Biol.* **2,** 62–69
52. Pasquale, E. B. (2008) Eph-ephrin bidirectional signaling in physiology and disease. *Cell* **133,** 38–52
53. Rothe, M., Sarma, V., Dixit, V. M., and Goeddel, D. V. (1995) TRAF2-mediated activation of NF-kappa B by TNF receptor 2 and CD40. *Science* **269,** 1424–1427
54. Pasquale, E. B. (2010) Eph receptors and ephrins in cancer: bidirectional signaling and beyond. *Nat. Rev. Cancer* **10,** 165–180
55. Walker-Daniels, J., Riese, D. J., and Kinch, M. S. (2002) c-Cbl-dependent EphA2 protein degradation is induced by ligand binding. *Mol. Cancer Res. MCR* **1,** 79–87
56. Take, H., Watanabe, S., Takeda, K., Yu, Z. X., Iwata, N., and Kajigaya, S. (2000) Cloning and characterization of a novel adaptor protein, CIN85, that interacts with c-Cbl. *Biochem. Biophys. Res. Commun.* **268,** 321–328
57. Raymond, B., Young, J. C., Pallett, M., Endres, R. G., Clements, A., and Frankel, G. (2013) Subversion of trafficking, apoptosis, and innate immunity by type III secretion system effectors. *Trends Microbiol.* **21,** 430–441
58. Ravichandran, V., Chawla, A., and Roche, P. A. (1996) Identification of a novel syntaxin- and synaptobrevin/VAMP-binding protein, SNAP-23, expressed in non-neuronal tissues. *J. Biol. Chem.* **271,** 13300–13303
59. Horii, M., Shibata, H., Kobayashi, R., Katoh, K., Yorikawa, C., Yasuda, J., and Maki, M. (2006) CHMP7, a novel ESCRT-III-related protein, associates with CHMP4b and functions in the endosomal sorting pathway. *Biochem. J.* **400,** 23–32
60. Thomas, D. D. H., Frey, C. L., Messenger, S. W., August, B. K., and Groblewski, G. E. (2010) A role for tumor protein TPD52 phosphorylation in endo-membrane trafficking during cytokinesis. *Biochem. Biophys. Res. Commun.* **402,** 583–587
61. Ungewickell, E., and Branton, D. (1981) Assembly units of clathrin coats. *Nature* **289,** 420–422
62. Mammoto, A., Ohtsuka, T., Hotta, I., Sasaki, T., and Takai, Y. (1999) Rab11BP/Rabphilin-11, a downstream target of rab11 small G protein implicated in vesicle recycling. *J. Biol. Chem.* **274,** 25517–25524
63. Aspenström, P. (1997) A Cdc42 target protein with homology to the non-kinase domain of FER has a potential role in regulating the actin cytoskeleton. *Curr. Biol. CB* **7,** 479–487
64. Hu, J., Troglio, F., Mukhopadhyay, A., Everingham, S., Kwok, E., Scita, G., and Craig, A. W. B. (2009) F-BAR-containing adaptor CIP4 localizes to early endosomes and regulates Epidermal Growth Factor Receptor trafficking and downregulation. *Cell. Signal.* **21,** 1686–1697
65. Arbuzova, A., Schmitz, A. A. P., and Vergères, G. (2002) Cross-talk unfolded: MARCKS proteins. *Biochem. J.* **362,** 1–12
66. Havrylov, S., Redowicz, M. J., and Buchman, V. L. (2010) Emerging roles of Ruk/CIN85 in vesicle-mediated transport, adhesion, migration, and malignancy. *Traffic Cph. Den.* **11,** 721–731
67. Goosney, D. L., DeVinney, R., and Finlay, B. B. (2001) Recruitment of cytoskeletal and signaling proteins to enteropathogenic and enterohemorrhagic Escherichia coli pedestals. *Infect. Immun.* **69,** 3315–3322
68. Arber, S., Barbayannis, F. A., Hanser, H., Schneider, C., Stanyon, C. A., Bernard, O., and Caroni, P. (1998) Regulation of actin dynamics through phosphorylation of cofilin by LIM-kinase. *Nature* **393,** 805–809
69. Mostowy, S., Nam Tham, T., Danckaert, A., Guadagnini, S., Boisson-Dupuis, S., Pizarro-Cerdá, J., and Cossart, P. (2009) Septins regulate bacterial entry into host cells. *PloS One* **4,** e4196
70. Mostowy, S., and Cossart, P. (2009) Cytoskeleton rearrangements during Listeria infection: clathrin and septins as new players in the game. *Cell Motil. Cytoskeleton* **66,** 816–823
71. Mostowy, S., and Cossart, P. (2012) Septins: the fourth component of the cytoskeleton. *Nat. Rev. Mol. Cell Biol.* **13,** 183–194
72. McIlhatton, M. A., Burrows, J. F., Donaghy, P. G., Chanduloy, S., Johnston, P. G., and Russell, S. E. (2001) Genomic organization, complex splicing pattern, and expression of a human septin gene on chromosome 17q25.3. *Oncogene* **20,** 5930–5939
73. Sellin, M. E., Stenmark, S., and Gullberg, M. (2012) Mammalian SEPT9 isoforms direct microtubule-dependent arrangements of septin core heteromers. *Mol. Biol. Cell* **23,** 4242–4255
74. Hardwidge, P. R., Rodriguez-Escudero, I., Goode, D., Donohoe, S., Eng, J., Goodlett, D. R., Aebersold, R., and Finlay, B. B. (2004) Proteomic analysis of the intestinal epithelial cell response to enteropathogenic Escherichia coli. *J. Biol. Chem.* **279,** 20127–20136
75. Mazurkiewicz, P., Thomas, J., Thompson, J. A., Liu, M., Arbibe, L., Sansonetti, P., and Holden, D. W. (2008) SpvC is a Salmonella effector with phosphothreonine lyase activity on host mitogen-activated protein kinases. *Mol. Microbiol.* **67,** 1371–1383
76. Li, H., Xu, H., Zhou, Y., Zhang, J., Long, C., Li, S., Chen, S., Zhou, J.-M., and Shao, F. (2007) The phosphothreonine lyase activity of a bacterial type III effector family. *Science* **315,** 1000–1003
77. Tang, P., Sutherland, C. L., Gold, M. R., and Finlay, B. B. (1998) Listeria monocytogenes invasion of epithelial cells requires the MEK-1/ERK-2 mitogen-activated protein kinase pathway. *Infect. Immun.* **66,** 1106–1112
78. Hobbie, S., Chen, L. M., Davis, R. J., and Galán, J. E. (1997) Involvement of mitogen-activated protein kinase pathways in the nuclear responses and cytokine production induced by Salmonella typhimurium in cultured intestinal epithelial cells. *J. Immunol.* **159,** 5550–5559
79. Sham, H. P., Shames, S. R., Croxen, M. A., Ma, C., Chan, J. M., Khan, M. A., Wickham, M. E., Deng, W., Finlay, B. B., and Vallance, B. A. (2011) Attaching and effacing bacterial effector NleC suppresses epithelial inflammatory responses by inhibiting NF-κB and p38 mitogen-activated protein kinase activation. *Infect. Immun.* **79,** 3552–3562
80. Krachler, A. M., Woolery, A. R., and Orth, K. (2011) Manipulation of kinase signaling by bacterial pathogens. *J. Cell Biol.* **195,** 1083–1092
81. Gao, X., Wang, X., Pham, T. H., Feuerbacher, L. A., Lubos, M.-L., Huang, M., Olsen, R., Mushegian, A., Slawson, C., and Hardwidge, P. R. (2013) NleB, a bacterial effector with glycosyltransferase activity, targets GAPDH function to inhibit NF-κB activation. *Cell Host Microbe* **13,** 87–99
82. Ruchaud-Sparagano, M.-H., Mühlen, S., Dean, P., and Kenny, B. (2011) The enteropathogenic E. coli (EPEC) Tir effector inhibits NF-κB activity by targeting TNFα receptor-associated factors. *PLoS Pathog.* **7,** e1002414
83. Berger, C. N., Crepin, V. F., Jepson, M. A., Arbeloa, A., and Frankel, G. (2009) The mechanisms used by enteropathogenic Escherichia coli to control filopodia dynamics. *Cell. Microbiol.* **11,** 309–322
84. Kenny, B., Ellis, S., Leard, A. D., Warawa, J., Mellor, H., and Jepson, M. A. (2002) Co-ordinate regulation of distinct host cell signaling pathways by multifunctional enteropathogenic Escherichia coli effector molecules. *Mol. Microbiol.* **44,** 1095–1107
85. Stokoe, D., Engel, K., Campbell, D. G., Cohen, P., and Gaestel, M. (1992) Identification of MAPKAP kinase 2 as a major enzyme responsible for the phosphorylation of the small mammalian heat shock proteins. *FEBS Lett.* **313,** 307–313
86. Lavoie, J. N., Hickey, E., Weber, L. A., and Landry, J. (1993) Modulation of actin microfilament dynamics and fluid phase pinocytosis by phosphorylation of heat shock protein 27. *J. Biol. Chem.* **268,** 24210–24214
87. Hernández-Rodríguez, Y., and Momany, M. (2012) Posttranslational modifications and assembly of septin heteropolymers and higher-order structures. *Curr. Opin. Microbiol.* **15,** 660–668
88. Garcia, G., Bertin, A., Li, Z., Song, Y., McMurray, M. A., Thorner, J., and Nogales, E. (2011) Subunit-dependent modulation of septin assembly: budding yeast septin Shs1 promotes ring and gauze formation. *J. Cell Biol.* **195,** 993–1004
89. Estey, M. P., Di Ciano-Oliveira, C., Froese, C. D., Fung, K. Y. Y., Steels, J. D., Litchfield, D. W., and Trimble, W. S. (2013) Mitotic regulation of SEPT9 protein by cyclin-dependent kinase 1 (Cdk1) and Pin1 protein is important for the completion of cytokinesis. *J. Biol. Chem.* **288,** 30075–30086
90. Gaidos, G., Soni, S., Oswald, D. J., Toselli, P. A., and Kirsch, K. H. (2007) Structure and function analysis of the CMS/CIN85 protein family identi-

fies actin-bundling properties and heterotypic-complex formation. *J. Cell Sci.* **120,** 2366–2377
91. Nakahira, M., Macedo, J. N. A., Seraphim, T. V., Cavalcante, N., Souza, T. A. C. B., Damalio, J. C. P., Reyes, L. F., Assmann, E. M., Alborghetti, M. R., Garratt, R. C., Araujo, A. P. U., Zanchin, N. I. T., Barbosa, J. A. R. G., and Kobarg, J. (2010) A draft of the human septin interactome. *PloS One* **5,** e13799
92. Mostowy, S., Bonazzi, M., Hamon, M. A., Tham, T. N., Mallet, A., Lelek, M., Gouin, E., Demangel, C., Brosch, R., Zimmer, C., Sartori, A., Kinoshita, M., Lecuit, M., and Cossart, P. (2010) Entrapment of intracytosolic bacteria by septin cage-like structures. *Cell Host Microbe* **8,** 433–444